Chemical Science

ROYAL SOCIETY OF CHEMISTRY

EDGE ARTICLE

View Article Online
View Journal | View Issue



Cite this: *Chem. Sci.*, 2025, **16**, 7773

All publication charges for this article have been paid for by the Royal Society of Chemistry

# Metal–silicon triple bonds: reactivity of the silylidyne complexes [Cp*(CO)$_2$M≡Si–Tbb] (M = Cr – W)†

Kanishk Tomer, Gregor Schnakenburg, Ujjal Das and Alexander C. Filippou *

Received 10th February 2025
Accepted 23rd March 2025

DOI: 10.1039/d5sc01063b

rsc.li/chemical-science

The different reactivity pattern of M≡Si and M≡C bonds (M = transition metal) is illustrated by a series of reactions of the silylidyne complexes [Cp*(CO)$_2$M≡Si–Tbb] (**1-M**) (M = Cr – W; Cp* = $\eta^5$-pentamethylcyclopentadienyl; Tbb = 4-*tert*-butyl-2,6-bis(bis(trimethylsilyl)methyl)phenyl)). Complexes **1-M** were obtained selectively from Li[Cp*M(CO)$_3$] and the 1,2-dibromodisilene (*E*)-Tbb(Br)Si=Si(Br)Tbb. The reaction of **1-Mo** and **1-W** with two equivalents of mesityl isocyanate leads selectively to complex **2-Mo** and **2-W**, respectively, featuring a novel $\kappa^2$*O*,*O*-imidocarbonatosilyl ligand. Ring opening of ethyloxirane occurs rapidly with **1-Mo** and leads to the hydrido–enolatosilylidene complex **3-Mo** illustrating the Si-centered electrophilicity of the silylidyne complex. Trimethylsilyldiazomethane induces a cleavage of the Mo≡Si bond of **1-Mo** after a rapid double [2 + 1] cycloaddition of the terminal N-atom, resulting in the first silaamidinato complex **4-Mo**. In comparison, the reaction of **1-Mo** with mesityl azide gives, after $N_2$ elimination, the Mo–silaiminoacyl complex **5-Mo**. All compounds were fully characterized and the isomerism and dynamics of **3-Mo** in solution were analysed by a combination of spectroscopic and quantum-chemical studies.

## 1. Introduction

Transition metal carbyne complexes are an important class of organometallic compounds displaying a diverse reactivity highlighted in many review articles,[1–9] and a monography.[10] Numerous stoichiometric transformations of carbyne complexes have been accomplished since the landmark discovery of the first examples by E. O. Fischer *et al.* in 1973 (Fig. 1, **A**),[11] the most prominent one involving the metathetical exchange of triple bonds, which culminated in the design of well-defined catalysts for the metathesis of alkynes,[7–9] with applications in total synthesis, polymer chemistry and supramolecular chemistry.[12–15] In comparison to carbyne complexes, isolation of group 14 heavier element analogs of the general formula L$_n$M≡E–R (M = transition metal, *E* = Si – Pb) is far more challenging given the reluctance of the Si – Pb to form one and even more so two π-bonds at the expense of σ-bonds for thermodynamic reasons. It requires fine stereoelectronic tuning of the metal fragment L$_n$M and kinetic stabilization of the M≡E functionality by a bulky substituent R to prevent uncontrollable follow-up reactions of the targeted compounds, such as head-to-tail cyclooligomerizations or unselective σ-bond activations.[16–18] Therefore it is not surprising that it took more than 20 years after E. O. Fischer's publication for the first germylidyne complex to be isolated by P. Power *et al.* taking advantage of the specific steric protection provided by a *m*-terphenyl substituent (Fig. 1, **C**).[19–21] Following this report, numerous group 6 germylidyne complexes[22–26] and first complexes featuring metal–tin[27–29] and metal–lead triple bonds[30–32] (Fig. 1, **D**) were obtained in our group using a $N_2$ or $PMe_3$ elimination method that proved to be significant for the development of this field.[18,33–35] Isolation of compounds featuring a metal–silicon triple bond was an uphill task due to the anomalous low electronegativity of silicon[36] and the lack of suitable sources for the SiR (silylidyne) fragment.[17]

Pioneering work of T. D. Tilley *et al.* on transition metal silyl and silylene complexes led to complexes containing base-stabilized silylidyne ligands.[37,38] The breakthrough came with the isolation of NHC-stabilized silicon(II) halides[39–43] and 1,2-dihalodisilenes[44–47] which were used in our group as selective electrophiles in reactions with electron-rich metal complexes to access stepwise or directly first neutral and cationic group 6 silylidyne complexes[48–52] (Fig. 1, **B**; Fig. 2, **G** and **H**) and then to transfer this approach to other transition metals[16,18,53–56] expanding considerably the scope of this chemistry (Fig. 2, **E**, **F**, **I** and **J**).

Another method to form metal-silicon triple bonds was developed by T. D. Tilley and H. Tobita and H. Hashimoto *et al.*

*Institut für Anorganische Chemie, Universität Bonn, Gerhard-Domagk-Str. 1, Bonn, 53121, Germany. E-mail: filippou@uni-bonn.de*

† Electronic supplementary information (ESI) available. CCDC 2421358–2421365. For ESI and crystallographic data in CIF or other electronic format see DOI: https://doi.org/10.1039/d5sc01063b

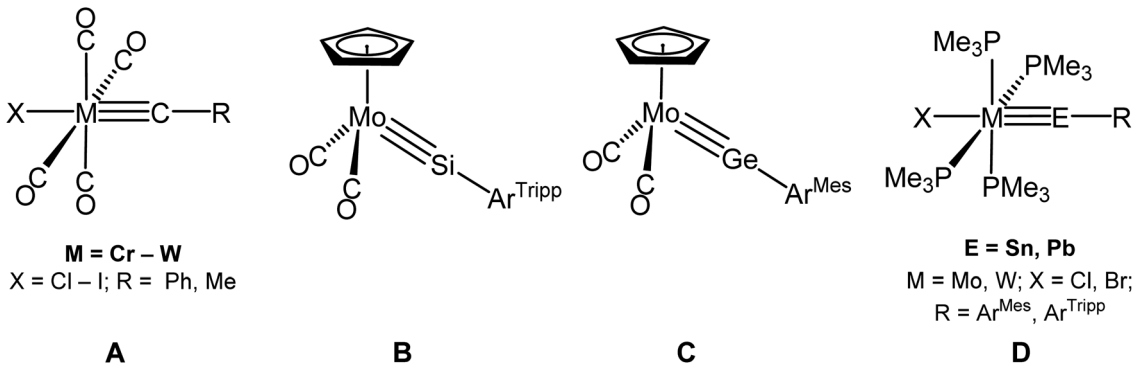


Fig. 1 First reported complexes featuring metal–tetrel triple bonds; $Ar^{Tripp} = C_6H_3$-2,6-$Tripp_2$, Tripp = 2,4,6-triisopropylphenyl; $Ar^{Mes} = C_6H_3$-2,6-$Mes_2$, Mes = 2,4,6-trimethylphenyl.

involving a stepwise metal-centered dehydrogenation of trihydridosilanes, which led to a first group 8 silylidyne complex, $[Cp^*(P^iPr_3)(H)Os{\equiv}Si{-}Tripp]^+$,[57] and the group 6 metal silylidyne complexes $[Cp^*(CO)_2M{\equiv}Si{-}R]$ (M = Cr – W; R = $C(SiMe_3)_3$, Eind), respectively.[58–61]

Silylidyne complexes have a similar electronic structure as Fischer-type carbyne complexes according to quantum chemical analyses.[18,62,63] However, the charge distribution along the M≡E bond differs significantly from that of Fischer carbyne complexes with the silicon atom carrying a high positive partial charge, whereas the carbyne–carbon is nearly electroneutral or carries a slight negative partial charge.[18] Also the M≡Si triple bonds are more polar than the M≡C bonds.[64] The increased polarity of the M≡Si triple bonds ($M^{(\delta-)}$–$Si^{(\delta+)}$) and the high silicon-centered electrophilicity provide a rationale for the high and distinct reactivity of the silylidyne complexes compared to that of the isovalent carbyne complexes. This is illustrated in Fig. 3 using a series of reactions studied in our group shortly after the synthesis of the silylidyne complex **B** in 2010.[49,51,65,66] For example, fast single and double additions of anionic nucleophiles at the electrophilic Si atom gave anionic silylidene complexes **K** and dianionic silyl complexes **L** respectively,[66] and

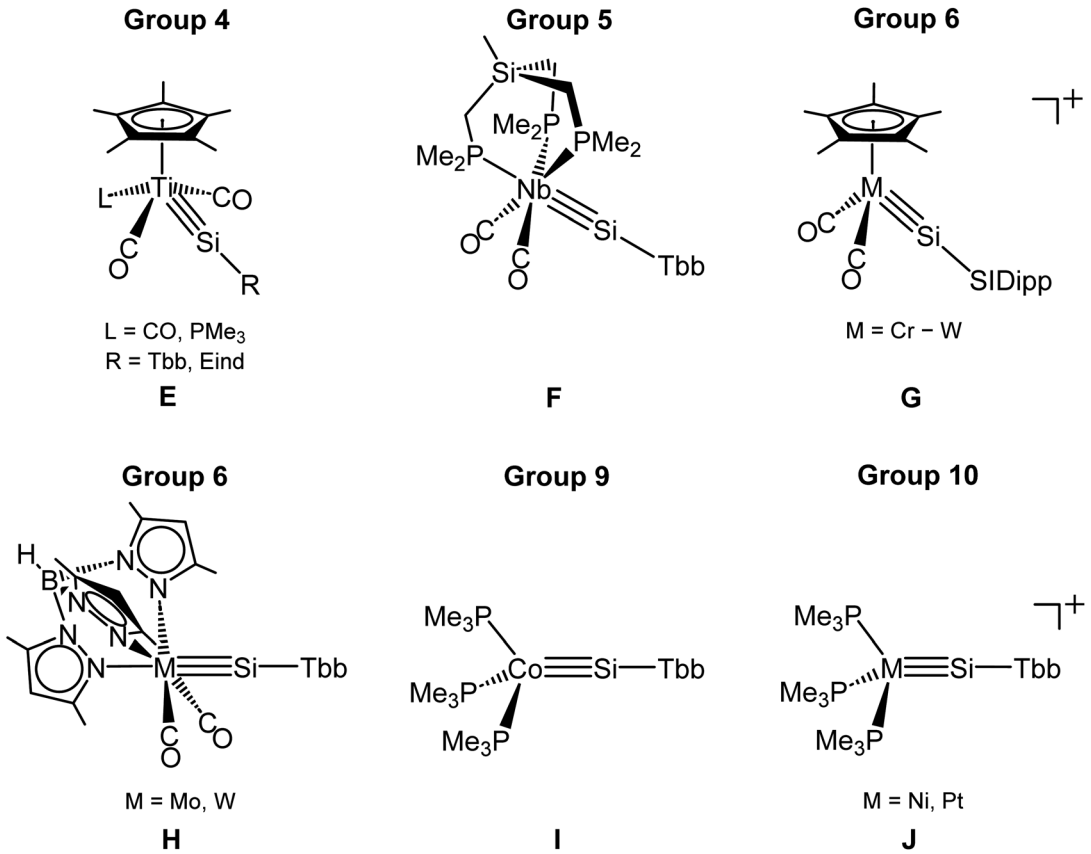


Fig. 2 Silylidyne complexes of various transition metal groups isolated and fully characterized in our group; SIDipp = $C[N(Dipp)CH_2]_2$, Dipp = 2,6-diisopropylphenyl; Tbb = $C_6H_2$-2,6-$(CH(SiMe_3)_2)_2$-4-*t*Bu; Eind = 1,1,3,3,5,5,7,7-$Et_8$-*s*-hydrindacene-4-yl.

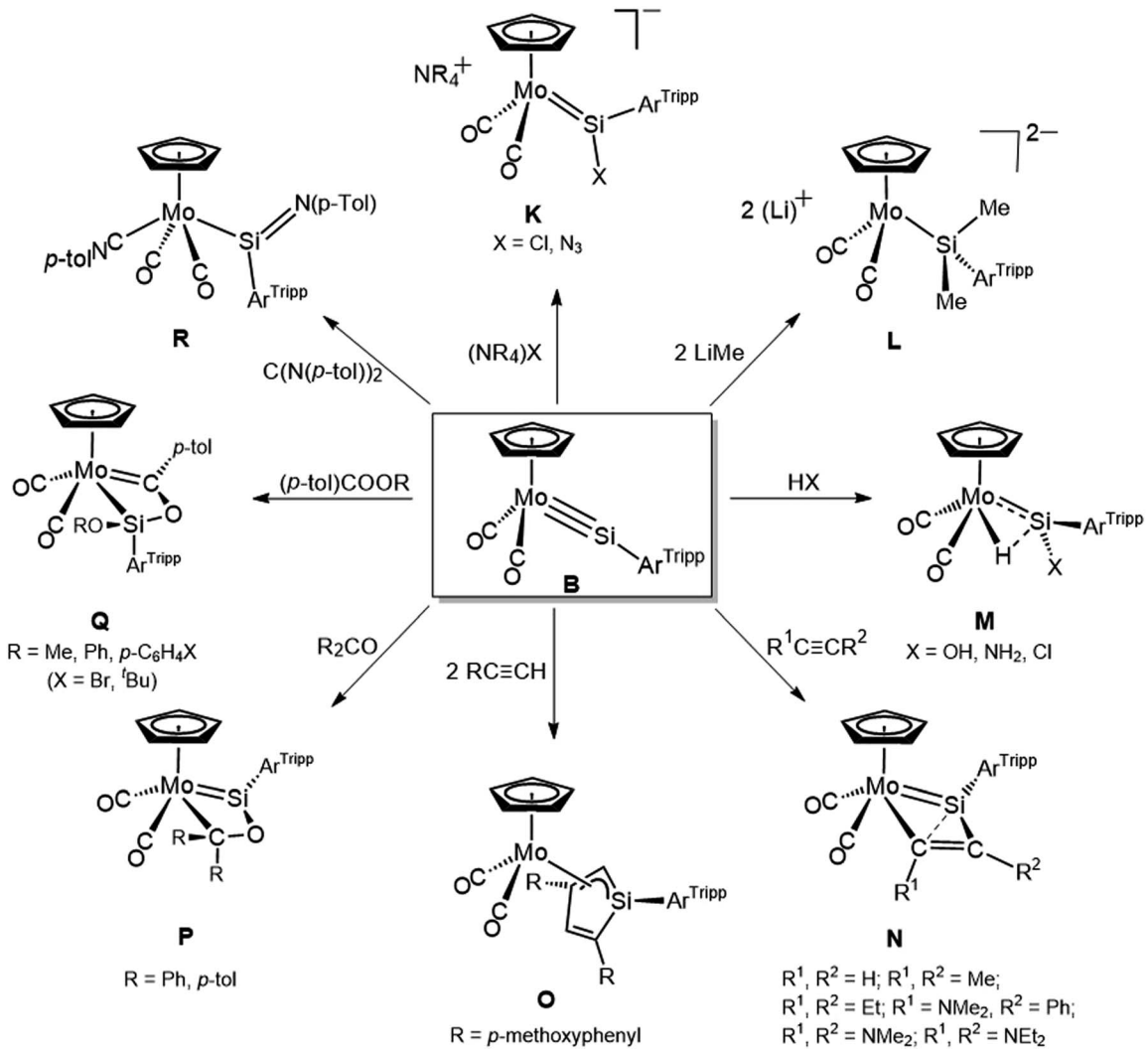


Fig. 3 Various reactions of the silylidyne complex **B** studied from 2010 to 2012 in our group.

regioselective 1,2-addition reactions of **B** with $H_2O$, $NH_3$ and HCl yielded the silylidene–hydrido complexes **M** featuring a M–H···Si bonding interaction (Fig. 3).[49] In comparison, reactions of the isovalent carbyne complexes $[(\eta^5\text{-}C_5R^1{}_5)(CO)_2M{\equiv}C\text{–}R^2]$ (M = Mo, W; $R^1$ = H, Me; $R^2$ = Me, Ph, $NEt_2$) with hydrogen halides show the opposed regioselectivity[67] leading to secondary carbene or $\eta^2$-acyl complexes, after single or double protonation of the carbyne carbon, respectively,[68–70] and reactions of Fischer type carbyne complexes with $H_2O$ or $NH_3$ have not been reported so far.

Remarkably, complex **B** rapidly undergoes [2 + 2] cycloadditions with various alkynes affording selectively the 1,2-metallasilacyclobutadienes **N**, which can further react with alkynes to give the $\eta^3$-*Si*,*C*,*C*-silacyclopentadienyl complexes **O** (Fig. 3). In comparison, reactions of the isovalent carbyne complexes $[(\eta^5\text{-}C_5R^1{}_5)(CO)_2M{\equiv}C\text{–}R^2]$ (M = Mo, W; $R^1$ = H, Me; $R^2$ = Me, Ph, $NEt_2$) with alkynes are not known, and in general the outcome of reactions of Fischer-type carbyne complexes with alkynes is unpredictable leading to different products such as alkyne polymers,[71] phenols,[72] alkyne(carbyne) complexes[73] or carbyne–alkyne–carbonyl coupling products.[74,75]

Complex **B** also reacts rapidly with carbonyl compounds. The [2 + 2] cycloadditions products **P** are formed regioselectively with ketones, whereas with esters the metalacyclic carbene complexes **Q** are obtained presumably *via* [2 + 2] cycloaddition followed by migration of the OR substituent from the carbonyl–carbon to the silicon atom (Fig. 3). In comparison, no reactions of Fischer-type carbyne complexes with carbonyl compounds have been reported so far, and Schrock-type carbyne complexes, which contain a nucleophilic carbyne–carbon and an electrophilic metal center, undergo Wittig-type reactions with aldehydes, ketones and esters yielding oxo–vinyl complexes.[76] It is noteworthy, that the latter reactions exhibit the opposite regioselectivity to those of **B** and lead to $C_{carbyne}$–$C_{carbonyl}$ coupling products.

Finally, reaction of silylidyne complex **B** with the carbodiimide (*p*-Tol)N=C=N(*p*-Tol) was found to give the iminosilyl (silaiminoacyl) complex **R** after [2 + 2] cycloaddition followed by cycloreversion (Fig. 3). In this case, the behaviour of **B** also differs from that of carbyne complexes[77] due to the metal$^{(\delta-)}$–silicon$^{(\delta+)}$ bond polarity.

Interesting reactivity patterns as presented above for **B** have been encovered later for the osmium complex $[Cp^*(P^iPr_3)(H)Os{\equiv}Si–Tripp]^+$ by T. D. Tilley *et al.*[57] and the group 6 metal silylidyne complexes $[Cp^*(CO)_2M{\equiv}Si–R]$ by H. Tobita and H. Hashimoto *et al.*,[58–60,78] and recently even the photochemical H–H and benzene C–H bond activation by $[Cp^*(CO)_2Cr{\equiv}Si–Eind]$ was reported confirming the high reactivity of silylidyne complexes.[61]

In the present work, the different reactivity pattern of M≡Si and M≡C bonds is exemplified by a series of reactions of the silylidyne complexes $[Cp^*(CO)_2M{\equiv}Si–Tbb]$ (**1-M**: M = Cr – W) with isocyanates, oxiranes, diazoalkanes and organic azides leading to complexes with novel Si-based ligands.

## 2. Results and discussion

### 2.1 Synthesis and characterization of the silylidyne complexes 1-M (1-M: M = Cr – W)

Complex **1-Mo** was obtained upon heating of a 1 : 2 mixture of the 1,2-dibromodisilene (*E*)-Tbb(Br)Si=Si(Br)Tbb and Li$[Cp^*Mo(CO)_3]$ in toluene at 110 °C for 4 hours. Monitoring of the reaction by $^1$H NMR and IR spectroscopy revealed the selective formation of the silylidyne complex **1-Mo**, which after workup was isolated in 68% yield as an air-sensitive, orange-red, thermally stable solid melting at 174 °C (eqn (1)).

Heating of (*E*)-Tbb(Br)Si=Si(Br)Tbb with the metallate Li$[Cp^*Mo(CO)_2(PMe_3)]$ in toluene at 110 °C also yielded **1-Mo** after $PMe_3$ elimination. In this case, conversion is faster and is completed in 30 min, but is less selective leading according to IR and NMR spectroscopy to a 10 : 1 mixture of **1-Mo** and the silylidyne complex $[Cp^*(CO)(PMe_3)Mo{\equiv}Si–Tbb]$ (**1-Mo-PMe$_3$**) (eqn (2)). The two products were separated after several crystallizations from *n*-pentane and **1-Mo** isolated in pure form, albeit in low yield (23%).

For comparison reasons, the chromium and tungsten silylidyne complexes $[Cp^*(CO)_2M{\equiv}Si–Tbb]$ (**1-Cr** (M = Cr); **1-W** (M = W)) were also obtained selectively from (*E*)-Tbb(Br)Si=Si(Br)Tbb and Li$[Cp^*M(CO)_3]$ in toluene at 110 °C (eqn (1)). **1-Cr** and **1-W** were isolated as very air-sensitive, dark-brown and orange-red solids in 66% and 56% yields, respectively (eqn (1)). Like **1-Mo**, both compounds are thermally stable solids and melt at 168 and 182 °C, respectively. Complexes **1-M** were fully characterized and their molecular structures determined by single-crystal X-ray diffraction (Fig. 4).

Selected bonding parameters and spectroscopic data of **1-M** and related group 6 metal silylidyne complexes previously characterized in our group,[49,51,52,79,80] are summarized in Table 1 for comparison with those of analogous carbyne complexes.[81–87]

The three-legged piano–stool complexes **1-M** are essentially $C_s$ symmetric with the symmetry plane bisecting the $Cp^*M(CO)_2$ fragment and passing through the aryl plane of the Tbb group, as evidenced by the twist angle $\theta$ between the aryl plane of the

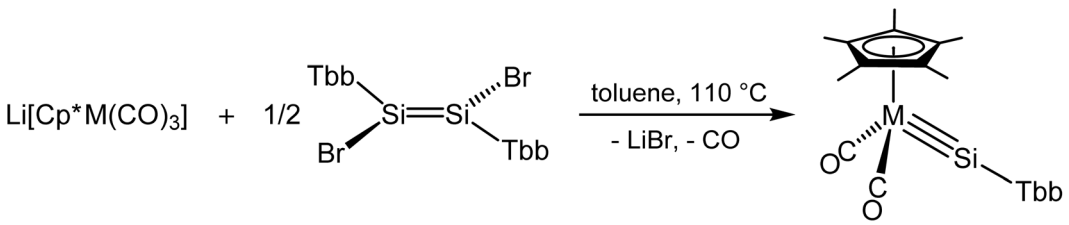


**1-M** (1)

M = Cr - W; Tbb = $C_6H_2$-2,6-$(CH(SiMe_3)_2)_2$-4-*t*Bu, Cp* = $\eta^5$-$C_5Me_5$

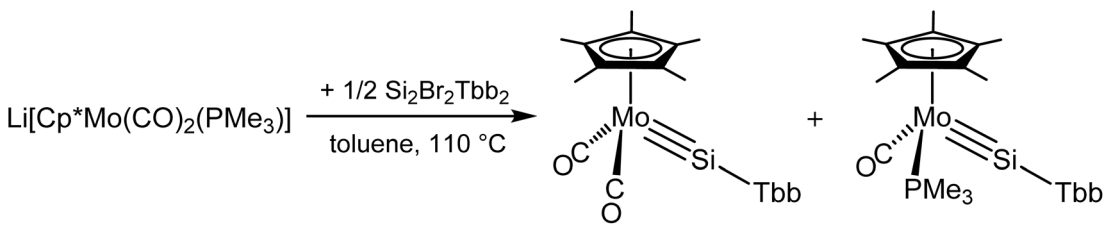


**1-Mo** : **1-Mo-PMe$_3$** (2)

10 : 1

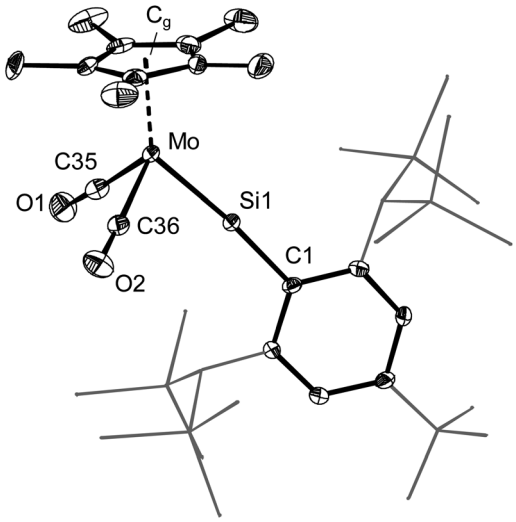


Fig. 4 DIAMOND plot of the molecular structure of **1-Mo**. Thermal ellipsoids are set at 50% probability, hydrogen atoms are omitted and the substituents of the Tbb group are presented as wireframe for the sake of clarity. Selected bond lengths (pm) and bond angles (°) for **1-Mo** (bond lengths and bond angles of **1-W** are given in square brackets): Mo–Si1 223.2(1) [224.55(6)], Mo–C35 197.0(4) [195.7(3)], Mo–C36 196.2(4) [196.7(3)], Si1–C1 185.6(3) [185.1(2)], Mo–Si1–C1 174.3(1) [174.88(8)], Si1–Mo–C35 89.1(1) [89.42(7)], Si1–Mo–C36 86.8(1) [86.97(7)], C35–Mo–C36 87.9(2) [88.5(1)], Si1–Mo–C$_g$ 135.86(7) [135.86(2)], C35–Mo–C$_g$ 122.2(1) [120.74(7)], C36–Mo–C$_g$ 121.2(1) [120.98(7)]; C$_g$ is the Cp* ring centroid.

Tbb substituent and the plane defined by the atoms Si, Mo and C$_g$ ($\theta$ = 1.7(1)° (**1-Mo**), 1.91(7)° (**1-W**); C$_g$ is the Cp* ring centroid) (Fig. 4).

All complexes feature very short metal–silicon bonds and almost linearly coordinated silicon centers with M–Si–C$_{Tbb}$ bond angles of 170.4–174.9° (Fig. 4 and Table 1). In fact, the Cr–Si distance of **1-Cr** (210.3(2) pm) is the shortest reported so far for a Cr–Si bond,[42] and is slightly shorter than those of the neutral silylidyne complexes [Cp*(CO)$_2$Cr≡Si–Eind] (211.51(4) pm) and [Cp*(CO)(PMe$_3$)Cr≡Si–Eind] (212.0(1) pm)[61] or the cationic silylidyne complex [Cp*(CO)$_2$Cr≡Si–SIDipp]B(Ar$^F$)$_4$ ($d$(Cr≡Si) = 212.20(9) pm; SIdipp = C[N(Dipp)CH$_2$]$_2$ (Dipp = 2,6-diisopropylphenyl), Ar$^F$ = C$_6$H$_3$-3,5-(CF$_3$)$_2$).[50] The M≡Si bond lengths of **1-Mo** (223.2(1) pm) and **1-W** (224.55(6) pm) are slightly longer than those of the neutral silylidyne complexes [Cp(CO)$_2$Mo≡Si–Ar$^{Tripp}$] (222.41(7) pm)[48] and [Cp*(CO)$_2$W≡Si–C(SiMe$_3$)$_3$] (222.97(9) pm) respectively,[58] and also slightly longer than those of the cationic silylidyne complexes [Cp*(CO)$_2$-M≡Si–SIDipp]B(Ar$^F$)$_4$ ($d$(Mo≡Si) = 222.12(9) pm; $d$(W≡Si) = 222.4(3) pm), but shorter than those of the Tp′ analogs (Table 1).[49,51] A further comparison shows that the Cr≡Si bond lengths are 10–14 pm shorter than the M≡Si bonds (M = Mo, W), the value comparing well with the difference of the triple-bond covalent radii $r_3$ of the elements ($r_3$(Cr) = 103 pm, $r_3$(Mo) = 113 pm; $r_3$(W) = 115 pm), reported by P. Pyykkö.[88] Notably, the Cr≡Si bond length of **1-Cr** (210.7 pm) and the Mo≡Si bond length of **1-Mo** (223.2 pm) are considerably shorter than the sum of the triple bond radii $r_{Cr}$ + $r_{Si}$ (219.95 pm) and $r_{Mo}$ + $r_{Si}$

Table 1 Selected spectroscopic and structural parameters of group 6 metal silylidyne complexes isolated in our group (top) and of isovalent carbyne complexes (bottom)

Silylidyne complexes

| Entry | Complex | $\nu$(CO) (cm$^{-1}$)[b,c] | $\delta$($^{29}$Si) (ppm)[d,e] | $d$(M≡Si) (pm) | ∠(M≡Si–C) (°) | Ref. |
|---|---|---|---|---|---|---|
| 1 | [Cp*(CO)$_2$Cr≡Si–Tbb] (**1-Cr**) | 1906, 1847[b] | 299.9[d] | 210.3(2) | 170.4(2) | This work |
| 2 | [Cp*(CO)$_2$Mo≡Si–Tbb] (**1-Mo**) | 1916, 1854[b] | 308.9[d] | 223.2(1) | 174.3(1) | This work |
| 3 | [Cp*(CO)$_2$W≡Si–Tbb] (**1-W**) | 1911, 1848[b] | 314.0[d] ($^1J$($^{183}$W,$^{29}$Si) = 316 Hz) | 224.55(6) | 174.88(8) | This work |
| 4 | [Cp*(CO)$_2$Cr≡Si–SIDipp]$^+$A$^-$ [a] | 1966, 1912[c] | 127.8[e] | 212.20(9) | 169.76(9) | 49 and 51 |
| 5 | [Cp*(CO)$_2$Mo≡Si–SIDipp]$^+$A$^-$ [a] | 1973, 1915[c] | 148.3[e] | 222.12(9) | 174.2(1) | 49 and 51 |
| 6 | [Cp*(CO)$_2$W≡Si–SIDipp]$^+$A$^-$ [a] | 1968, 1906[c] | 178.2[e] ($^1J$($^{183}$W,$^{29}$Si) = 420 Hz) | 222.4(3) | 172.1(3) | 51 |
| 7 | [Tp′(CO)$_2$Mo≡Si–Tbb] | 1912, 1836[b] | 258.5[d] | 226.14(9)[f]<br>225.43(9) | 160.8(1)[f]<br>158.5(1) | 52 |
| 8 | [Tp′(CO)$_2$W≡Si–Tbb] | 1901, 1823[b] | 259.8[d] ($^1J$($^{183}$W,$^{29}$Si) = 272 Hz) | 227.06(8)[f]<br>226.37(8) | 161.7(1)[f]<br>159.5(1) | 79 and 80 |

Carbyne complexes

| Entry | Complex | $\nu$(CO) (cm$^{-1}$)[g,h,i,j] | $\delta$(M≡*C*) (ppm)[k,l,m,n,o,p] | $d$(M≡C) (pm) | ∠(M≡C–C) (°) | Ref. |
|---|---|---|---|---|---|---|
| 9 | [Cp(CO)$_2$Cr≡C–Ph] | 1991, 1922[g] | 325.7[k] | 170.5(2) | 175.5(2) | 81 |
| 10 | [Cp(CO)$_2$Mo≡C–Ph] | 1996, 1922[g] | 309.4[l] | — | — | 82 |
| 11 | [Cp(CO)$_2$W≡C–Ph] | 1984, 1905[g] | 299.3[m] | — | — | 83 |
| 12 | [Cp(CO)$_2$W≡C–(*p*-tol)] | 1990, 1919[h] | 300.1[n] | 182(2) | 176(2) | 84 |
| 13 | [Cp*(CO)$_2$Cr≡C–Ph] | 1984, 1921[i] | 323.7[k] | — | — | 81 |
| 14 | [Cp*(CO)$_2$W≡C–(*p*-tol)] | 1981, 1910[h] | 301.3[o] | — | — | 85 |
| 15 | [Tp′(CO)$_2$Mo≡C–(*p*-tol)] | 1982, 1899[j] | 288.9[p] | 180.4(4) | 163.1(3) | 86 |
| 16 | [Tp′(CO)$_2$W≡C–(*p*-tol)] | 1974, 1888[h] | 279.6[q] | 182.9(3) | 163.2(3) | 87 |

[a] A$^-$ = B(C$_6$H$_3$-3,5-(CF$_3$)$_2$)$_4^-$. [b] In toluene. [c] In PhF. [d] In ($D_6$)benzene. [e] In ($D_5$)chlorobenzene. [f] Bonding parameters of the two independent molecules found in the crystal lattice. [g] In $CH_2Cl_2$. [h] In *n*-hexane. [i] In *n*-pentane. [j] In thf. [k] In $CD_2Cl_2$ at −40 °C. [l] In $CD_2Cl_2$ at −50 °C. [m] In $CD_2Cl_2$ at −20 °C. [n] In $CD_2Cl_2$ at −30 °C. [o] In $CD_2Cl_2$/$CH_2Cl_2$ at r.t. [p] In $CDCl_3$ at r.t. [q] In $CD_2Cl_2$ at r.t.

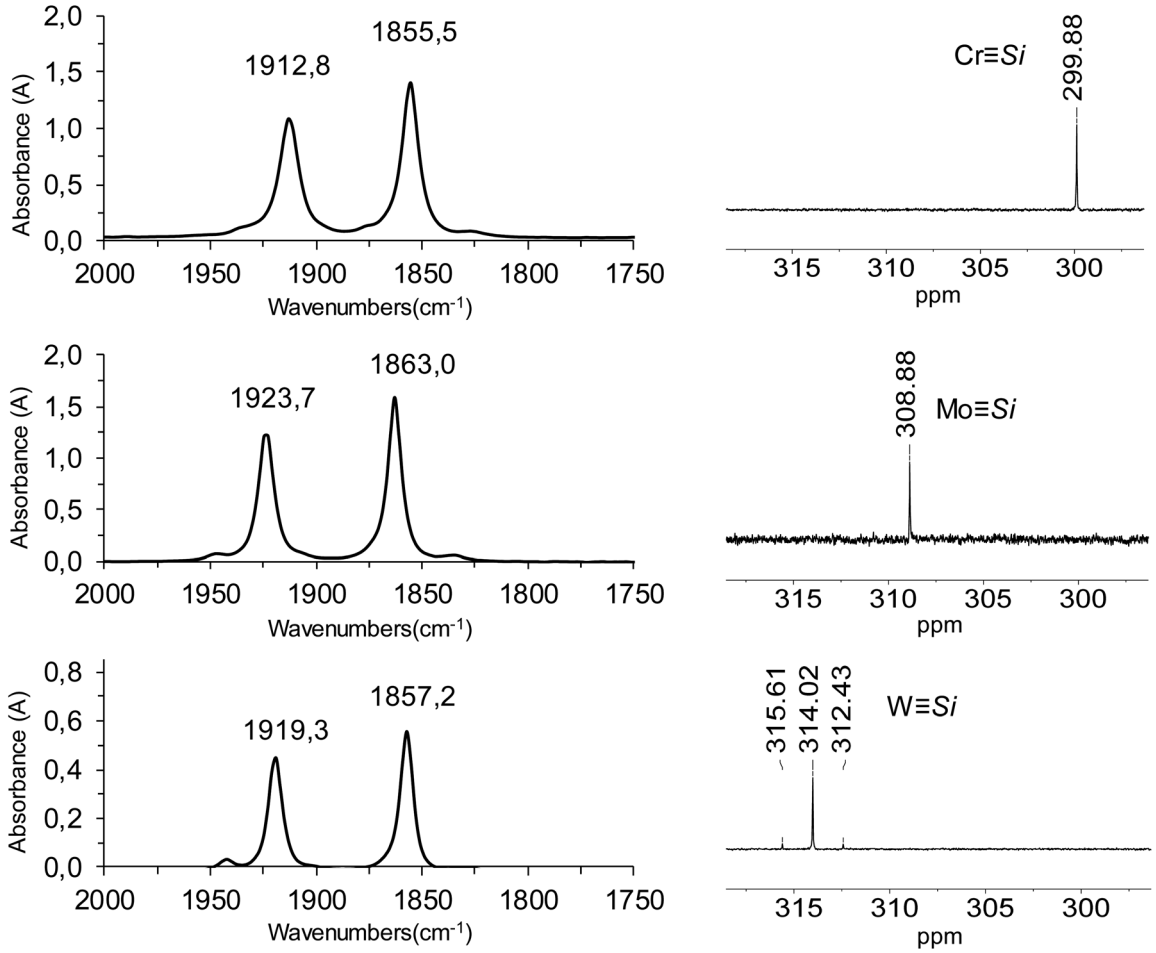


Fig. 5 (left) FT-IR spectra of the silylidyne complexes **1-Cr** – **1-W** in *n*-hexane in the spectral range 2000–1750 $cm^{-1}$ showing the two $\nu$(CO) absorption bands; (right) $^{29}Si\{^{1}H\}$ NMR spectra (99.36 MHz) of **1-Cr** – **1-W** in ($D_6$)benzene at 298 K showing the M≡*Si* signals.

(229.45 pm), which are derived from the experimental M≡M bond lengths of $Cp^*_2M_2(CO)_4$ ($d$(Cr≡Cr) = 228.0(2) pm;[89] $d$(Mo≡Mo) = 248.8(3) pm[90]) and the Si≡Si bond length of $Si_2Tbb_2$ ($d$(Si≡Si) = 210.1(1) pm)[91] using the equations $r_M = d(M{\equiv}M)/2$ and $r_{Si} = d(Si{\equiv}Si)/2$, respectively. This bond shortening can be explained by the increased polarity and strength of the M≡Si bonds of **1-M** (M = Cr, Mo).

The IR spectra of complexes **1-Cr** – **1-W** display two intense absorption bands, which are typical for *cis*-dicarbonyl complexes and are assigned to the in-phase (A′ symmetric) and out-of-phase (A″ symmetric) CO stretching modes of the $C_s$-symmetric complexes (Fig. 5). The $\nu$(CO) absorption bands of the silylidyne complexes appear at considerably lower wavenumbers than those of the isovalent carbyne complexes (*cf.* entry 1 with 13, 3 with 14 or 7 with 15 in Table 1) indicating the much higher σ-donor/π-acceptor ratio of the silylidyne ligand SiR (R = Tbb) than that of the carbyne ligand CR (R = Ph, *p*-Tol). It should also be noted, that the $\nu$(CO) absorption bands of the silylidyne complexes **1-Mo** and **1-W** appear even at lower wavenumbers than those of the aminocarbyne complexes $Cp^*(CO)_2M{\equiv}CNEt_2$ (M = Mo, W).[92,93] In general, the $\nu$(CO) bands of the Cp* containing silylidyne complexes appear at higher wavenumbers than those of the Tp′analogues (*cf.* entry 2 with 7 or 3 with 8 in Table 1) and the $\nu$(CO) bands of the molybdenum silylidyne complexes at higher wavenumbers than those of their tungsten congeners (*cf.* entry 2 with 3 or 7 with 8 in Table 1). Notably, the same trends are observed in the isovalent carbyne complexes (*cf.* entry 14 with 16, 10 with 11 or 15 with 16 in Table 1) illustrating the stronger electron-donating ability of the Tp′ than the Cp* ligand in these systems[94] and the stronger W–CO than Mo–CO π-back bonding.[95]

The most distinctive NMR spectroscopic feature of the silylidyne complexes **1-M** (M = Cr – W) is the markedly deshielded $^{29}$Si (M≡*Si*) NMR signal, which moves from Cr ($\delta$ = 299.9 ppm) → Mo ($\delta$ = 308.9 ppm) → W ($\delta$ = 314.0 ppm) stepwise to lower field (Fig. 5). It is noteworthy, that the isovalent carbyne complexes $Cp(CO)_2M{\equiv}CPh$ do also exhibit a very deshielded $^{13}$C (M≡*C*) NMR signal, which, however, moves from Cr ($\delta$ = 325.7 ppm) → Mo ($\delta$ = 309.4 ppm) → W ($\delta$ = 299.3 ppm) in the opposite direction, *i.e.* to higher field (Table 1). Interestingly, the $^{29}$Si (M≡*Si*) NMR signals of **1-Mo** and **1-W** appear at lower field than those of their Tp′ analogs (*cf.* entry 2 with 7 and 3 with 8 in Table 1) and the same trend is observed for the related Cp/Cp* and Tp′ containing carbyne complexes (*cf.* entry 10 with 15 and 14 with 16 in Table 1). All tungsten silylidyne complexes

have much larger $^1J(^{183}W–^{29}Si)$ coupling constants than tungsten silyl complexes including **2-W** (*vide infra*).

### 2.2 Reactions of silylidyne complexes with isocyanates and oxiranes

Complexes **1-Mo** and **1-W** react slowly with two equivalents of mesityl isocyanate in toluene at 80 °C to exclusively give complexes **2-Mo** and **2-W** (eqn (3)). No intermediates were detected by IR or NMR spectroscopy in these reactions leading exclusively to the *trans* isomers. In comparison, complex **1-Cr** does not react with MesNCO even after prolonged heating in toluene at 110 °C, the shorter Cr≡Si bond being apparently too sterically protected by the Cp* ligand and the Tbb substituent.

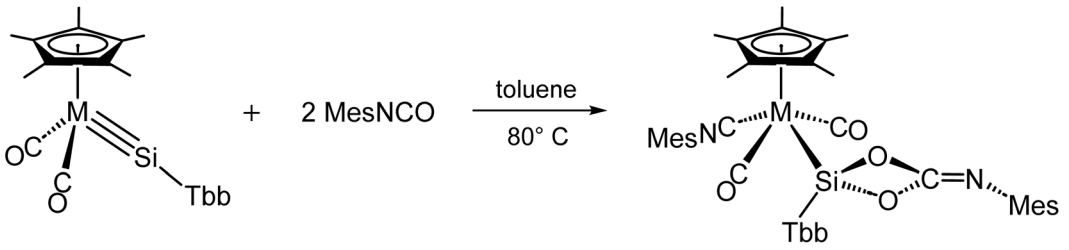


**1-M** **2-M** (3)

M = Mo, W; Mes = $C_6H_2$-2,4,6-$Me_3$

Complexes **2-Mo** and **2-W** were isolated as air-sensitive, creamy-white and white solids in 85 and 89% yields, respectively. Both compounds are thermally stable and decompose upon melting at 227 and 228 °C, respectively. Complexes **2-Mo** and **2-W** were fully characterized and their molecular structures determined by X-ray diffraction (Fig. 6).

The "four-legged piano-stool" complexes feature a novel silyl ligand containing a $\kappa^2O,O$-bonded imidocarbonato substituent. Complexes **2-M** can therefore be regarded as cyclic silyl esters of the unknown *N*-mesityl-imidocarbonic acid $C(=NMes)(OH)_2$. Imidocarbonates $\{C(=NR)(OR)_2\}$ are in general less known[96–100] than their structural isomers $C(=O)(NR_2)(OR)$ (carbamates),[101] and only two silyl esters related to **2-M** have been reported so far.[102,103] The 1,3-dioxasiletane ring formed by the imidocarbonato substituent is planar and the Si–O, C–O, C=N bond lengths and inner angles of the ring (O–Si–O, O–C–O, Si–O–C) compare very well with those of the compound $Si(O_2CNDipp)\{C(SiMe_3)_2CH_2\}_2$ obtained from the silylene $Si\{C(SiMe_3)_2CH_2\}_2$ and DippNCO.[102] The M–Si bond lengths of **2-Mo** (253.01(7) pm) and **2-W** (253.5(1) pm) are *ca.* 30 pm longer than the M≡Si bond lengths of **1-Mo** and **1-W**, but are in good agreement with the median value of the Mo–Si (254.2 pm) and W–Si single bond lengths (255.6 pm) of all structurally characterized complexes to date.[104]

The IR spectra of **2-Mo** and **2-W** in toluene solution display two characteristic absorption bands at 1710/1692 $cm^{-1}$ and 1710/1694 $cm^{-1}$ respectively, which are assigned to the $\nu(O_2CN)$ stretching modes of the imidocarbonato susbstituent (ESI, Fig. S24 and S43†). In addition, the IR spectra show one absorption band for the C≡N stretching mode of the isocyanide ligand at 2103 $cm^{-1}$ (**1-Mo**) and 2097 $cm^{-1}$ (**1-W**) and two absorption bands for the in-phase and out-of-phase CO stretching modes of the carbonyl ligands at 1962 $cm^{-1}$ and 1901 $cm^{-1}$ (**1-Mo**) and 1954 $cm^{-1}$ and 1894 $cm^{-1}$ (**1-W**), respectively. The higher frequency $\nu$(CO) band is much less intense than the lower frequency $\nu$(CO) band, confirming the *trans* arrangement of the two CO ligands.[105,106]

A salient spectroscopic feature of **2-Mo** and **2-W** is the unusually deshielded $^{29}Si$ NMR signal, which appears at considerably lower field ($\delta$(**2-Mo**): 105.8 ppm, $\delta$(**2-W**): 88.6 ppm)

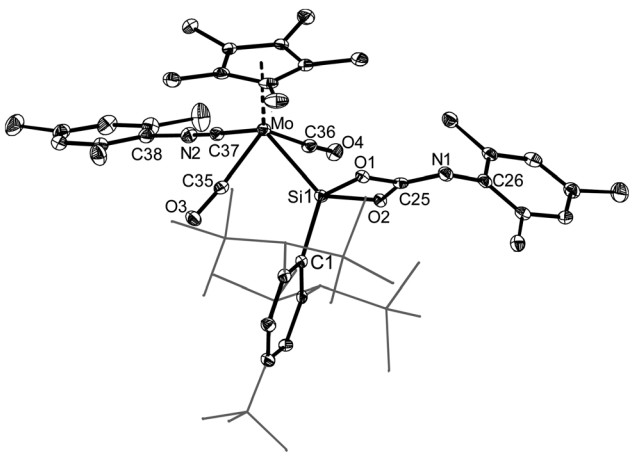


Fig. 6 DIAMOND plot of the molecular structure of **2-Mo**. Thermal ellipsoids are set at 30% probability, hydrogen atoms were omitted and the substituents of the Tbb group are presented as wireframe for the sake of clarity. Selected bond lengths (pm) and bond angles (°): for **2-Mo** (bond lengths and bond angles of **2-W** are given in square brackets): Mo–Si1 253.01(7) [253.5(1)], Mo–C35 198.8(3) [198.8(5)], Mo–C36 197.8(3) [197.2(5)], Mo–C37 204.2(3) [204.2(5)], Si1–O1 174.8(2) [175.4(3)], Si1–O2 176.0(2) [175.9(3)], Si1–C1 188.8(2) [187.9(4)], O1–C25 135.9(3) [135.6(5)], O2–C25 136.0(3) [136.6(5)], N1–C25 125.9(3) [125.7(5)], Si1–Mo–C35 74.11(7) [75.2(1)], Si1–Mo–C37 127.7(1) [128.4(1)], C35–Mo–C36 110.3(1) [111.6(2)], O1–Si1–O2 75.69(8) [75.7(1)], O1–C25–O2 104.6(2) [104.8(3)], Si1–O1–C25 90.1(1) [90.0(2)], Si1–O2–C25 89.5(1) [89.5(2)].

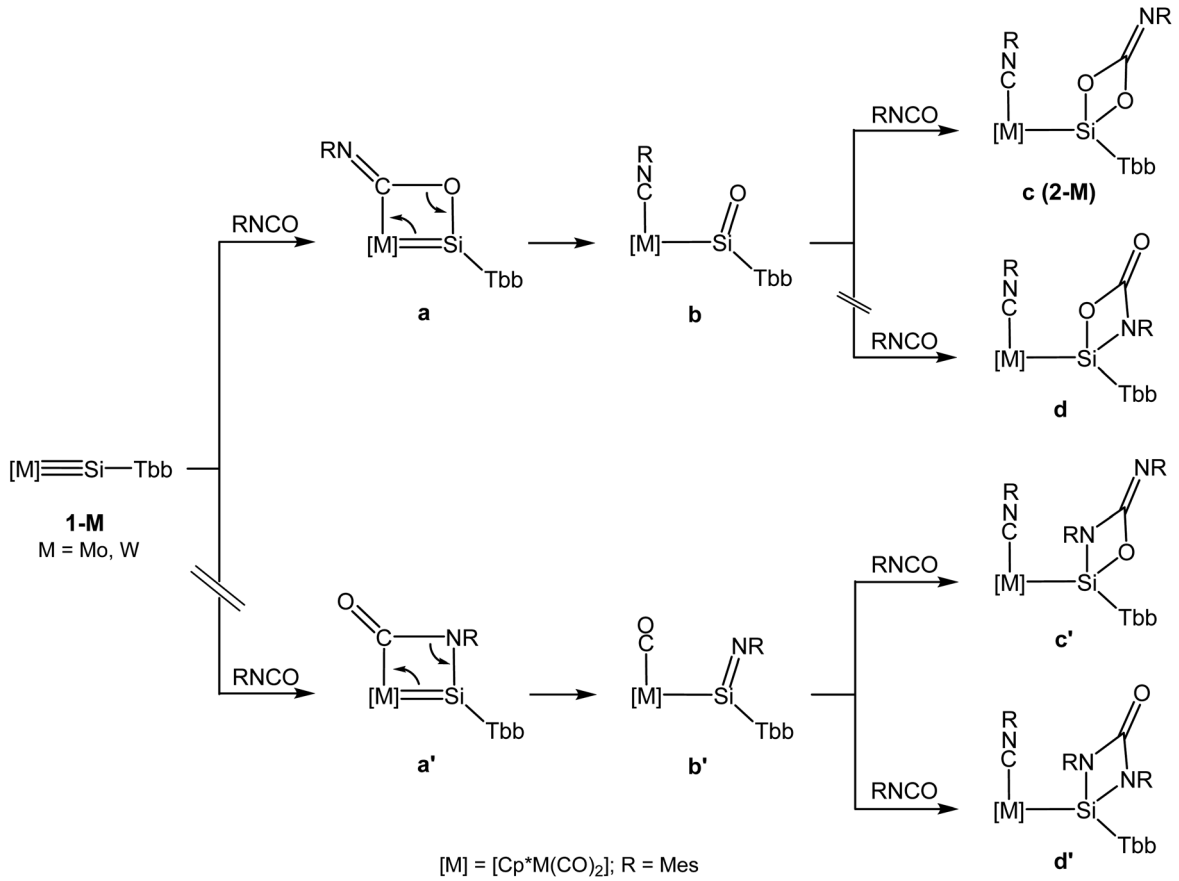


Fig. 7 Possible products **c**–**d′** of the reactions of **1-Mo** and **1-W** with MesNCO. Only **c** is observed showing the high chemo- and regioselectivity of these reactions.

than that of $Si(O_2CNDipp)\{C(SiMe_3)_2CH_2\}_2$ ($\delta$ = 53.4 ppm)[102] and of all other four-cordinate Si compounds with a four-membered siletane ring $Si(X^1)(X^2)C=Y$ ($X^1$, $X^2$, Y = NR, O) ($\delta$ = −90.9–53.4 ppm).[107] The $^{29}$Si NMR signal of **2-W** is flanked by a pair of $^{183}$W satellites resulting in a $^1J$(W–Si) coupling constant of 79.6 Hz, that is larger than those of other tungsten silyl complexes ($^1J$(W–Si) = 5–64 Hz),[108] but much smaller than that of **1-W** (316 Hz). The $^{13}C\{^1H\}$ NMR spectra of **2-Mo** and **2-W** ($(D_6)$benzene, 298 K) display characteristic NMR signals for the $CO_2$NMes carbons at 149.3 and 149.4 ppm, and for the isocyanide-carbons at 184.8 and 171.2 ppm, respectively (ESI, Chapter 2.4 and 2.5†). Notably, complexes **2-Mo** and **2-W** contain a stereogenic four-coordinate Si center due to the fixed orientation of the N-bonded Mes group, leading to two $^{13}$C NMR resonances for the *trans*-arranged CO ligands (ESI, Fig. S28 and S48†). In addition, rotation of the Tbb substituent about the Si–$C_{Tbb}$ bond is hindered on the NMR time scale and leads to diastereotopic *ortho* ($C^2$/$C^6$) and *meta* $C^3$/$C^5$ positions of the Tbb aryl ring and to a double set of $^1$H, $^{13}$C and $^{29}$Si NMR signals for the substituents at these positions, which were fully assigned by 2D NMR spectroscopy of **2-Mo** in ($D_8$)THF at 243 K (ESI, Fig. S25–S30†). A dynamic process sets on with increasing temperature leading to a site exchange of the diastereotopic CO ligands and the diastereotopic *ortho* and *meta* positions of the Tbb ring, as evidenced by the $^1$H and $^{13}$C NMR spectra of **2-Mo** in ($D_6$)benzene at 348 K (ESI, Fig. S37–S40†). The process leads to a racemization of **2-Mo** and occurs presumably *via* an inversion of the $N_{imido}$-bonded mesityl group. The Gibbs energy of activation ($\Delta G^{\ddagger}$ (298 K)) for this process was found to be approximately 60 kJ mol$^{-1}$, which compares well with the values obtained for the *N*-aryl imidocarbonates $(MeO)_2C{=}N(p\text{-}C_6H_4X)$ ($X$ = H, Cl, Me) ($E_a$ (in acetone) = 56.1–69.5 kJ mol$^{-1}$).[97]

Formation of **2-M** (M = Mo, W) can be explained by the three-step reaction sequence outlined in Fig. 7. The first step involves a [2 + 2] cycloaddition to give the 1,3,2-metallaoxasilacyclo-1-buten-4-imine **a**, which after ring opening gives the $\eta^1$-silaacyl-isocyanide complex **b**. Species **b** reacts with another equivalent of MesNCO to give the final product **2-M**. *cis–trans* isomerization may precede or follow the reaction of **b** with MesNCO leading finally only to the *trans*-isomer **2-M**.

No evidence was found for the formation of the putative products **d**, **c′** and **d′** (Fig. 7). This suggests that both [2 + 2] cycloaddition steps are highly chemoselective with the C=O bond of MesNCO being exclusively involved in the [2 + 2] cycloaddition with the M≡Si bond of **1-M** and then with the Si=O bond of **b** (Fig. 7). Both [2 + 2] cycloaddition steps are also highly regioselective with the O atom getting exclusively attached to the silicon atom, due to the high $M^{(\delta-)}{\equiv}Si^{(\delta+)}$ bond polarity of **1-M** and the $Si^{(\delta+)}=O^{(\delta-)}$ bond polarity of **b**. Notably, the Schrock-type neopentylidyne complex $[Cl_3(dme)W{\equiv}CtBu]$

undergoes with cyclohexylisocyanate (CyNCO) a Wittig-type $C_{carbyne}$–$C_{isocyanate}$ coupling reaction to give after ring-opening a tungsten imido-ketenyl intermediate, which then inserts a second equivalent of CyNCO into the W–$C_{ketenyl}$ bond to yield an oxaazetin tungstenacycle.[109] The opposite chemoselectivity and regioselectivity of the cycloaddition step in this reaction reflects the reversed polarity of the metal–carbon bonds of Schrock-type carbyne complexes ($M^{(\delta+)}{\equiv}C^{(\delta-)}$) and the metal–silicon bonds ($M^{(\delta-)}{\equiv}Si^{(\delta+)}$) of **1-M**.

The factors that favour an O- instead of an N-binding to silicon and lead exclusively to the C=O cycloaddition product in both steps (**1-M** → **a** and **b** → **2-M**) are subtle. In fact, reaction of MeNCO with the silylidene complex cation $[Cp^*(PMe_3)_2Ru = SiMe_2]^+$ shows the opposite chemoselectivity and leads exclusively to the [(C=N) + (Ru=Si)] cycloaddition product $[Cp^*(PMe_3)_2RuSiMe_2N(R)C{=}O]^+$.[110] Both reactants contain in this case sterically less demanding methyl groups at the isocyanate-nitrogen and silicon atoms. In contrast, reaction of the silylidene–hydrido complex [Cp*(CO)(H)Ru=Si(H)C(SiMe$_3$)$_3$], which contains a sterically demanding trisyl substituent at silicon, with MesNCO yields the C=O hydrosilylation product [Cp*(CO)Ru[$\eta^2$-N,Si–N(Mes) = C(H)OSi(H)C(SiMe$_3$)$_3$].[111] In this reaction, a precoordination of MesNCO *via* the O-atom to the electrophilic silylidene–silicon atom was proposed to be the first step based on quantum chemical studies.[112] It should also be noted, that protonation of HNCO in $FSO_3H/SO_2$ or MeNCO in the gas-phase occurs at the N-site.[113,114] In contrast, silylation of $SiMe_3NCO$ with $(SiMe_3)[B(C_6F_5)_4]$ occurs at the O-site to give $[SiMe_3NCOSiMe_3][B(C_6F_5)_4]$, where the N-silylated cation $[(SiMe_3)_2NCO]^+$ is almost isoenergetic.[115]

The electrophilicity of the Si center and the high polarity M≡Si in **1-M** let us presume that the silylidyne complexes would promote the ring opening of cyclic ethers. In fact, addition of ethyloxirane to an orange-red solution of **1-Mo** in *n*-hexane at room temperature was accompanied by a rapid color change to brownish-yellow to yield regioselectively the *cis*-(*E*-but-1-ene-1-olato)silylidene–hydrido complex **3-Mo** along with a minor Cp* containing component, which on the basis of its $^1$H NMR spectroscopic features is suggested to be the *Z*-stereoisomer **3-Mo′** (eqn (4)). The *E*/*Z* stereoisomers are formed in the molar ratio of 7 : 3. Conversion of **1-Mo** to **3-Mo**/**Mo′** is an unusual Lewis-acid promoted ring-opening reaction of an oxirane by α-elimination.[116] The oxirane is presumably activated upon O-coordination to the Lewis acidic Si center of **1-Mo** for the next step, which involves ring-opening after regioselective proton abstraction from the more acidic ring-$CH_2$ group by the basic molybdenum center. The reaction of **1-Mo** with ethyloxirane is reminiscent of the reaction of the hydrido–hydrosilylidene complex $[Cp^*(CO)_2(H)W{=}Si(H)\{C(SiMe_3)_3\}]$ with oxiranes,[117] whereas reactions of Fischer-type carbyne complexes with oxiranes have not yet been reported.

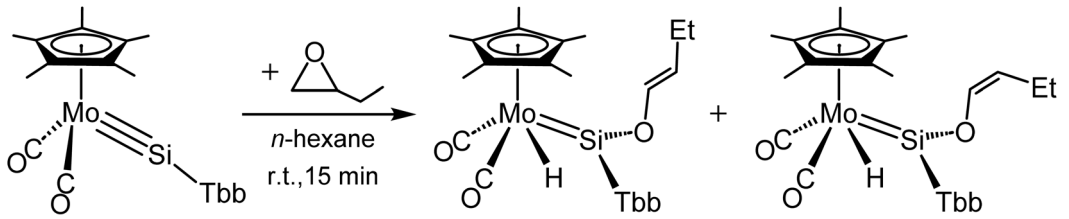


**1-Mo** **3-Mo** (*E*-isomer) **3-Mo′** (*Z*-isomer) (4)

After work-up **3-Mo** was isolated as an analytically pure, very air-sensitive, pale-yellow solid that melts with decomposition at 165 °C. Compound **3-Mo** is the first enolatosilylidene complex to be fully characterized and its structure was determined by single-crystal X-ray diffraction (Fig. 8).[118] **3-Mo** crystallizes in the non chiral space group *Pbca* and exists in the solid-state as a racemic mixture of the *C* (clockwise) and *A* (anticlockwise) enantiomers due to the presence of a crystallographic inversion center. The molecular structure of the *A* enantiomer is depicted in Fig. 8a and shows a "four-legged piano-stool" complex with a *cis*-arrangement of the two CO ligands (∠(CO–Mo–CO) = 84.9(3)°). The silylidene ligand is coordinated to the Mo center *via* a short Mo–Si bond (*d*(Mo=Si) = 235.8(2) pm), which compares well with that of the aminosilylidene complex $[Cp(CO)_2(H)Mo{=}Si(NH_2)Ar^{Tripp}]$ (*d*(Mo=Si) = 237.96(5) pm (**M**, Fig. 3),[49] and lies in the range found for other arylsilylidene complexes (*d*(Mo=Si) = 228.8(2)–238.72(7) pm).[38,48,60,66,119,120] The Mo=Si bond of **3-Mo** is considerably longer than the Mo≡Si bond of **1-Mo** (223.2(1) pm) and shorter than the Mo–Si single bond of **2-Mo** (253.01(7) pm). The silicon center is trigonal-planar coordinated with the Tbb ring plane lying orthogonal to the silicon coordination plane. The angles at silicon differ though markedly. The Mo–Si–$C_{Tbb}$ angle is widened to 135.4(2)° due to the steric demand of the Tbb substituent, whereas the O–Si–$C_{Tbb}$ angle is lowered to 100.0(3)° reflecting the low tendency of silicon to hybridize and the increased s character of the Si hybrid orbital involved in the Mo–Si σ bond. The silylidene ligand adopts a tilted conformation with the buten-1-ene-1-olato substituent pointing towards the Cp* ligand, as evidenced by the dihedral angle $C_g$–Mo–Si1–O1 of −46.2(3)° ($C_g$: Cp* ring centroid) (Fig. 8b). The hydrido

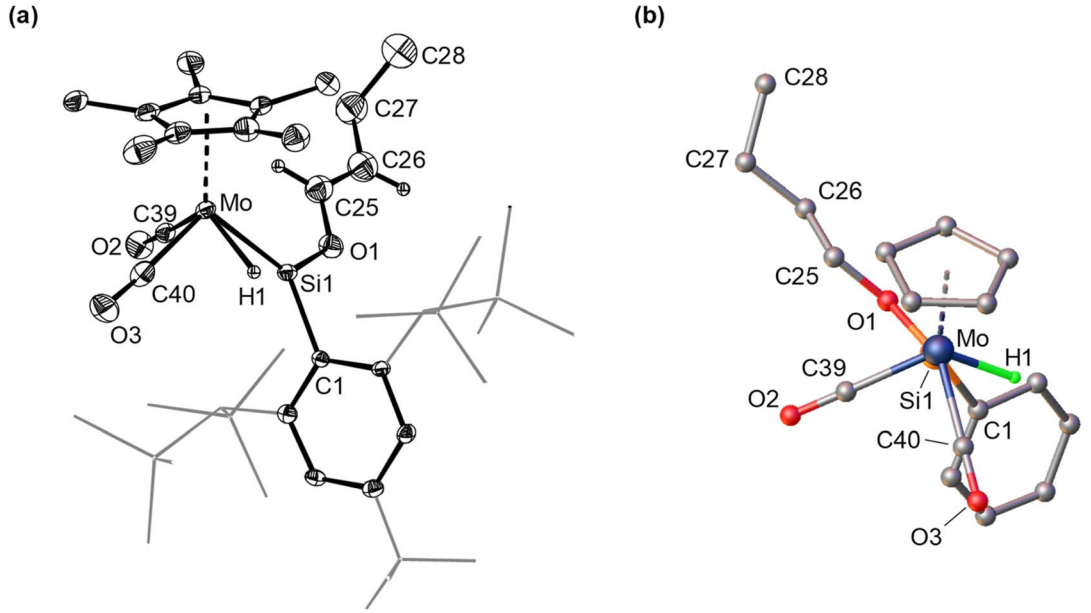


Fig. 8 (a) DIAMOND plot of the molecular structure of the *A* (anticlockwise) enantiomer of **3-Mo**.Thermal ellipsoids are set at 30% probability, hydrogen atoms were omitted except the Mo-bonded hydrogen atom and the substituents of the Tbb group are presented as wireframe for the sake of clarity. Selected distances (pm) and bond angles (°): for **3-Mo**: Mo–Si1 235.8(2), Mo–H1 181(7), Mo–C39 196.1(8), Mo–C40 197.8(8), Si1⋯H1 208(6), Si1–O1 164.7(5), Si1–C1 188.2(6), C25–O1 138(1), C25–C26 133.0(12), C26–C27 148.0(8), C27–C28 153(1), Si1–Mo–C39 75.4(2), Si1–Mo–C40 106.4(2), Si1–Mo–H 58.1(19), C39–Mo–C40 84.9(3), Mo–Si1–C1 135.4(2), Mo–Si1–O1 124.6(2), O1–Si1–C1 100.0(3), O1–C25–C26 121.3(8), C25–C26–C27 124.3(9). (b) View along the Mo–Si bond of **3-Mo** (Olex plot) showing the tilted conformation of the silylidene ligand and the anticlinal conformation of the Mo–H and Si–OR bonds (the methyl groups of the Cp* ligand and the substituents of the Tbb group were omitted for clarity).

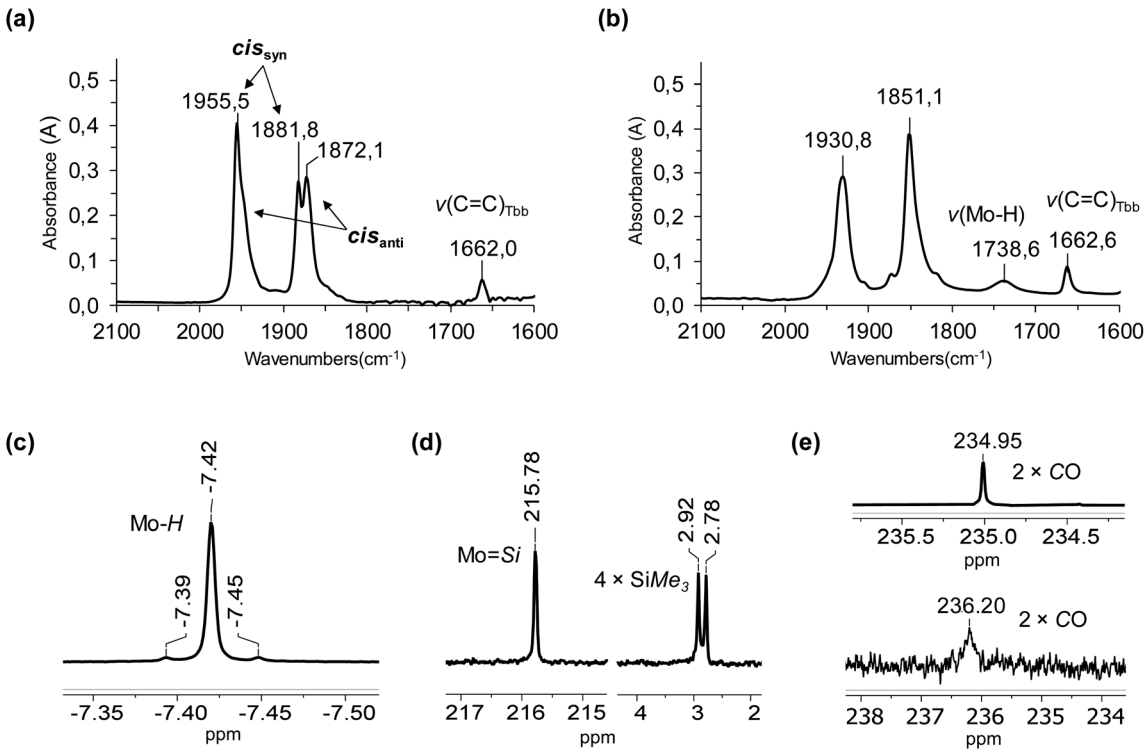


Fig. 9 (a) Solution IR spectrum of **3-Mo** in *n*-hexane in the spectral range 2100–1600 $cm^{-1}$. (b) ATR-IR spectrum of **3-Mo** in the spectral range 2100–1600 $cm^{-1}$. (c) Hydride NMR signal with its $^{29}Si$ satellites in the $^{1}H$ NMR spectrum of **3-Mo** in ($D_6$)benzene at 298 K. (d) $^{29}Si$ NMR spectrum of **3-Mo** in ($D_6$)benzene at 298 K. (e) (*top*) CO signal in the $^{13}C\{^{1}H\}$ NMR spectrum of **3-Mo** in ($D_6$)benzene at 298 K; (*bottom*) CO signal in the $^{13}C\{^{1}H\}$ NMR spectrum of **3-Mo** in ($D_8$)toluene at 193 K.

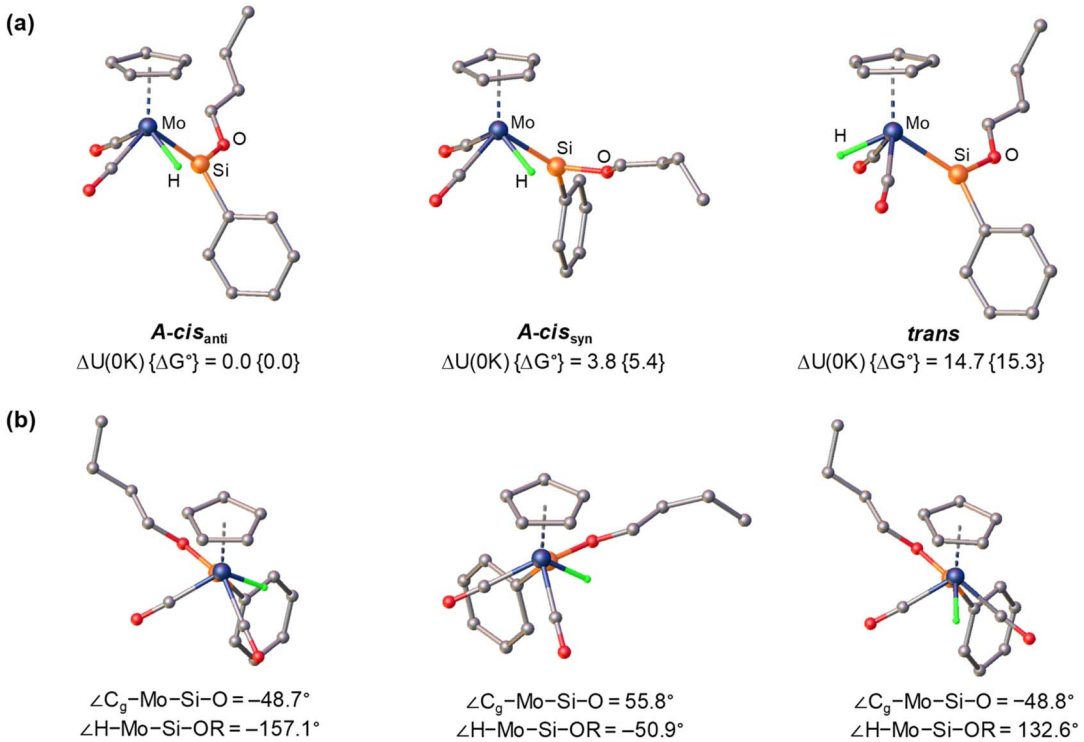


Fig. 10 (a) Side view of the calculated structures (Olex plots) of the isomers ***A*-cis**$_{anti}$, ***A*-cis**$_{syn}$ and ***trans*** of **3-Mo** with their relative zero-point vibrational energy corrected inner energies $\Delta U(0\ K)$ (kJ mol$^{-1}$) and standard Gibbs energies $\Delta G°$ (kJ mol$^{-1}$) (values in curly brackets); (b) view along the Mo–Si bond of the calculated structures of the isomers ***A*-cis**$_{anti}$, ***A*-cis**$_{syn}$ and ***trans*** (Olex plots) with values of the dihedral angles $C_g$–Mo–Si–O and H–Mo–Si–OR, respectively. The methyl groups of the Cp* ligand and the substituents of the Tbb group were omitted for clarity.

ligand was localized in the difference Fourier map in the vacant *cis*-coordination site relative to the silylidene ligand (∠(H1–Mo–Si1) = 58(2)°) at a distance of 181(7) pm and 208(6) pm from the molybdenum and Si1 atoms, respectively.

**2.2.1 Spectroscopic and quantum chemical studies on the isomerism and dynamics of the silylidene–hydrido complex 3-Mo.** Complex **3-Mo** shows interesting isomerism and dynamics in solution, which was investigated by a combination of IR and NMR spectroscopic studies with a detailed analysis of the potential energy surface (PES) (ESI, Chapter 4†). In fact, the molecular structure of **3-Mo** in the solid-state shows one isomer with two *cis*-ligated CO ligands. If one assumes, that only this *cis* isomer would be present in solution, then only two $\nu$(CO) bands of similar intensity would be expected in the IR spectrum of **3-Mo**, one at higher frequency arising from the in-phase stretching mode of the CO ligands and one at lower frequency originating from the out-of-phase stretching mode of the CO ligands.[106] However, the IR spectrum of **3-Mo** in *n*-hexane shows three clearly visible $\nu$(CO) bands at 1956, 1882 and 1872 cm$^{-1}$ as well as a shoulder on the low-frequency side of the band at 1956 cm$^{-1}$ indicating that an additional isomer of **3-Mo** must be present in solution (Fig. 9a).

This observation is in line with the results of quantum chemical studies suggesting the presence of two diastereomers at similar low energy, labeled as ***cis*$_{anti}$** and ***cis*$_{syn}$**, respectively. Both isomers have *cis*-ligated CO ligands, are present in solution as a racemic mixture of the *C* (clockwise) and *A* (anticlockwise) enantiomers, and display a tilted conformation of the silylidene ligand, with the Si-bonded OR substituent pointing towards the Cp* ring, as evidenced by the dihedral

Table 2 Selected experimental and calculated bond lengths, bond angles, twist angles and dihedral angles (°) of the *A* enantiomer of **3-Mo** (***A*-(3-Mo)**$_{exp}$: experimental values; ***A*-(3-Mo)**$_{th}$ = (***A*-cis**$_{anti}$): calculated values), and calculated bond angles, twist angles and dihedral angles (°) of the isomers ***A*-cis**$_{syn}$ and ***trans***

| | Mo–Si | Mo–H | Si···H | CO–Mo–CO | H–Mo–Si | $C_g$–Mo–H | $C_g$–Mo–Si | ΣSi[a] | TA1[b] | TA2[c] | DHA1[d] | DHA2[e] |
|---|---|---|---|---|---|---|---|---|---|---|---|---|
| ***A*-(3-Mo)$_{exp}$** | 235.8(2) | 181(7) | 208(6) | 84.9(3) | 58(2) | 120(2) | 131.4(1) | 360 | 45.2(2) | 31(3) | −46.2(3) | −150(3) |
| ***A*-cis$_{anti}$ (*A*-(3-Mo)$_{th}$)** | 236.1 | 173.1 | 209.1 | 85.3 | 59.1 | 121.9 | 127.8 | 360 | 48.5 | 22.0 | −48.7 | −157.1 |
| ***A*-cis$_{syn}$** | 236.6 | 175.0 | 195.9 | 82.4 | 54.4 | 122.3 | 126.5 | 359.8 | 53.6 | 52.2 | 55.8 | −50.9 |
| ***trans*** | 239.1 | 170.2 | 361.3 | 107.5 | 123.1 | 111.7 | 125.2 | 359.9 | 47.4 | 45.2 | −48.8 | 132.6 |

[a] Sum of the bond angles at the Mo-bonded silicon atom (Si). [b] Twist angle between the ($C_g$,Mo,Si)-plane ($C_g$: Cp* ring centroid) and the (O,Si,$C_{Tbb}$)-plane. [c] Twist angle between the (H,Mo,Si)-plane and the (O,Si,$C_{Tbb}$)-plane [d] Dihedral angle $C_g$–Mo–Si–O. [e] Dihedral angle H–Mo–Si–O.

angle $C_g$–Mo–Si–O of +48.7/−48.7° (***C/A-cis*$_{anti}$**) and −55.8°/+55.8° (***C/A-cis*$_{syn}$**), respectively (Fig. 10a). The isomers ***C/A-cis*$_{anti}$** and ***C/A-cis*$_{syn}$** differ though in the relative orientation of the silylidene and the hydrido ligand. In ***A-cis*$_{anti}$** the Mo–H and Si–OR groups adopt an anticlinal conformation (∠H–Mo–Si–OR = −157.1°), *i.e.* the Mo–H bond vector points almost in the opposite direction of the Si–OR bond vector, whereas in ***A-cis*$_{syn}$** the Mo–H and Si–OR groups have a synclinal conformation (∠H–Mo–Si–OR = −50.9°) (Fig. 10b). ***cis*$_{anti}$** is the most stable isomer with a slightly lower Gibbs energy of 5.4 kJ mol$^{-1}$ than the ***cis*$_{syn}$** isomer. In addition, a *trans*-configurated isomer, labeled as ***trans***, was found to be a local minimum on the PES, whose Gibbs energy is 15.3 kJ mol$^{-1}$ higher than the most stable isomer ***cis*$_{anti}$** (Fig. 10).

The calculated bond lengths and angles of ***cis*$_{anti}$** agree very well with the experimental bond lengths and bond angles of **3-Mo** and even the twist angles describing the twist of the silylidene ligand with respect to the Cp* and the hydrido ligand, respectively, or the $C_g$–Mo–Si–O dihedral angle, which describes the orientation of the OR substituent with respect to the Cp* ring, compare very well with the experimental values (Table 2).

Curve fitting and deconvolution of the IR spectrum using a Gaussian profile gave four bands peaking at 1956, 1950, 1883 and 1872 cm$^{-1}$ and their frequency integrated intensities (ESI, Fig. S88 and Table S5†). After comparison with the calculated harmonic frequencies of the ***cis*$_{anti}$** and ***cis*$_{syn}$** isomers, the bands at 1950 and 1872 cm$^{-1}$ were assigned to the in-phase and out-of-phase combination of the two CO stretching modes of the ***cis*$_{anti}$** isomer, and those at 1956 and 1883 cm$^{-1}$ to the in-phase and out-of-phase combination of the two CO stretching modes of the ***cis*$_{syn}$** isomer (Fig. 9a). The equilibrium constant $K_{exp} = \frac{c(cis_{anti})}{c(cis_{syn})}$ and the standard Gibbs energy difference $\Delta G^{\circ}_{exp}$ ($G^{o}$(***cis*$_{anti}$**) − $G$(***cis*$_{syn}$**)) at 298 K was estimated assuming that the sum of the frequency integrated intensities of the two $\nu$(CO) bands of the isomer ***cis*$_{anti}$** is equal to that of ***cis*$_{syn}$**. The obtained values ($K_{exp}$ = 2.6, $\Delta G^{\circ}_{exp}$ (298 K) = −2.4 kJ mol$^{-1}$) are in reasonable agreement with the calculated values ($K_{th}$ = 8.8, $\Delta G^{\circ}_{th}$ = −5.4 kJ mol$^{-1}$). From the Gibbs energy difference $\Delta G^{\circ}_{trans-cis}$ between the ***trans*** isomer and the ***cis*$_{anti}$** isomer at 298 K of 15.3 kJ mol$^{-1}$, the molar ratio $\frac{trans}{cis_{anti}}$ of 0.002 was obtained, indicating that the ***trans*** isomer does not contribute to the IR spectrum of **3-Mo** in solution due to its very low concentration.

The IR spectrum of **3-Mo** in *n*-hexane also shows one characteristic band arising from the C=C stretching mode of the but-1-ene-1-olato substituent at 1662 cm$^{-1}$ (Fig. 9a). In comparison, no band could be observed for the Mo–H stretching mode in solution, which is however clearly visible in the ATR-IR spectrum of **3-Mo** at 1739 cm$^{-1}$ (Fig. 9b). To rationalize this observation the relaxed potential energy surface around the minimum structure of ***cis*$_{anti}$** and ***cis*$_{syn}$** was calculated, varying the Mo–H distance from 1.6 to 2.0 Å and the Si–H distance from 1.6–2.2 Å (Fig. 11). The 2-dimensional surface plots show a shallow potential and an enhanced flexibility of the hydride around the respective minimum position. For example, a change of the Si–H distance from 1.9 to 2.2 Å and of the Mo–H distance from 1.7–1.8 Å leads to an increase of the electronic energy of ***cis*$_{anti}$** by maximal 2 kJ mol$^{-1}$. Therefore, one may assume that several rapidly equilibrating species are present in solution, whose energy differ by less than 2 kJ mol$^{-1}$ from the minimum structures ***cis*$_{anti}$** and ***cis*$_{syn}$** and whose Mo–H bond lengths and Si–H distances varying in a range of few pm around the values of the minimum structures of ***cis*$_{anti}$** and ***cis*$_{syn}$**, respectively. The positions of the $\nu$(CO) bands of these species are essentially the same as those of ***cis*$_{anti}$** and ***cis*$_{syn}$**, respectively, but their $\nu$(Mo–H) bands vary, as evidenced by a comparison of ***cis*$_{anti}$** and ***cis*$_{syn}$**, which shows that a shortening of the Mo–H bond by 2 pm (***cis*$_{syn}$** (175.0 pm) → ***cis*$_{anti}$** (173.1 pm)) leads to an increase of the $\nu$(Mo–H) frequency by 56 cm$^{-1}$ (***cis*$_{syn}$** (1735 cm$^{-1}$) → ***cis*$_{anti}$** (1791 cm$^{-1}$)). One may therefore conclude that the low intensity of the $\nu$(Mo–H) band of ***cis*$_{anti}$** and ***cis*$_{syn}$** is distributed over a larger wavenumber range around

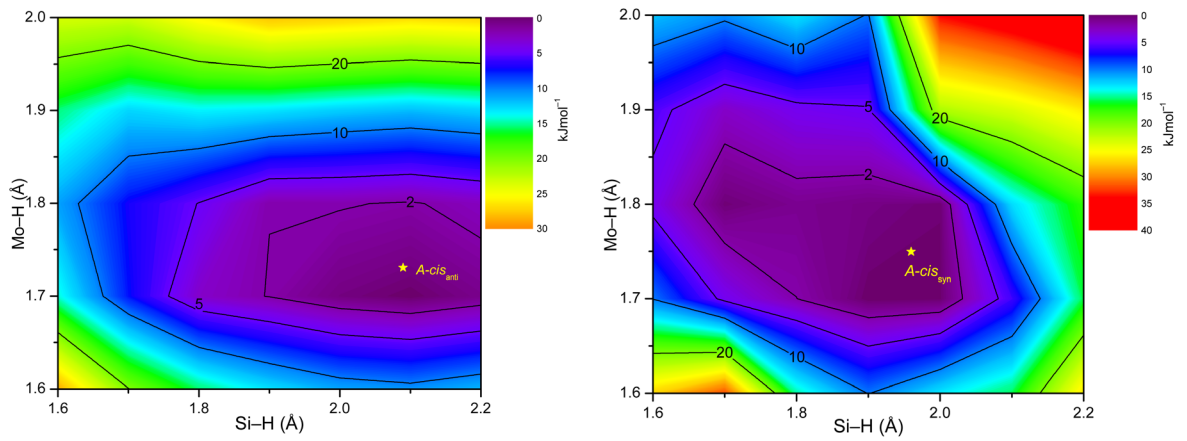


Fig. 11 Two-dimensional representation of the relaxed potential energy surface ***cis*$_{anti}$** (left) and ***cis*$_{syn}$** (right) as a function of the Si–H and Mo–H distance in Å (mesh width: 5 pm). Electronic energies are given in kJ mol$^{-1}$. The global (fully optimized) minimum (set to 0.0 kJ mol$^{-1}$) is depicted with a yellow star, respectively. Iso-energy lines at 2, 5, 10, and 20 kJ mol$^{-1}$ are drawn as black lines.

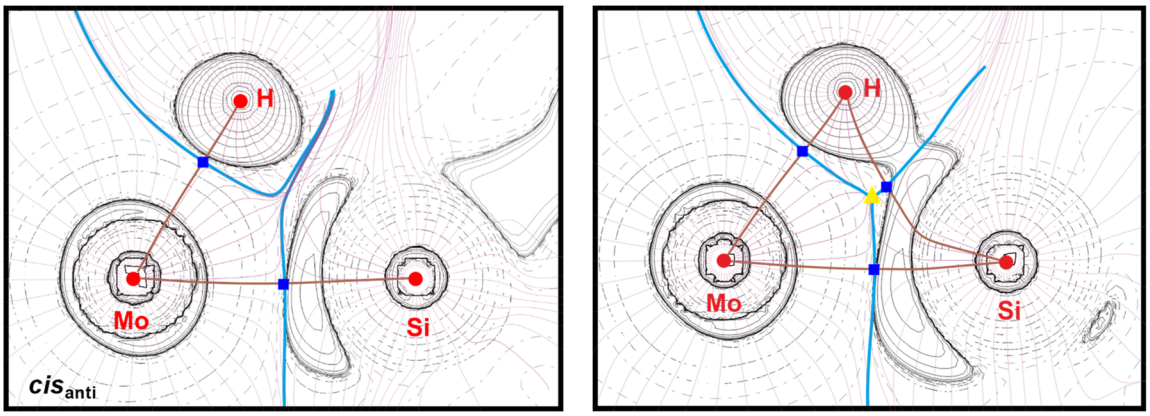


Fig. 12 Molecular graph of ***cis***$_{anti}$ (left) and ***cis***$_{syn}$ (right) showing core critical points (red circles), bond critical points (dark blue squares), ring critical points (yellow triangles), bond paths (brown lines), gradient paths (mauve lines, projected into the given plane), areas of charge concentration (solid hairlines) and charge depletion (broken hairlines) as well as interatomic surfaces (light blue lines).

the respective band maximum leading to a considerable broadening of the $\nu$(Mo–H) band in solution. This conclusion is confirmed by the close similarity of the Boltzmann corrected IR spectrum of the structural ensemble captured by the two PES scans with the experimental spectrum of **3-Mo** in *n*-hexane solution (ESI, Fig. S90†).

The computed Mo–H bond lengths of ***cis***$_{anti}$ (173.1 pm) and ***cis***$_{syn}$ (175.0 pm) lie in the range of Mo–H 2c–2e bond lengths ($d$(Mo–H) = 168.5(3)[121]–178.9(7)[122]) obtained from neutron diffraction studies. In comparison, the calculated Si–H distances of ***cis***$_{anti}$ (209.1 pm) and ***cis***$_{syn}$ (195.9 pm) are considerably longer than those obtained for 2c–2e Si–H bonds by neutron diffraction ($d$(Si–H) = 148.1(5)–150.6(2)).[123,124] The Si–H distances of ***cis***$_{anti}$ and ***cis***$_{syn}$ are much shorter than the sum of the van der Waals radii of Si and H (330 pm),[125] and appear in the range of distances for which non-classical M–H···Si interactions have been discussed.[126]

A topological analysis of the electron density of both isomers was carried out to address the question, whether a direct Si···H bonding interaction is present in ***cis***$_{anti}$ and ***cis***$_{syn}$. For ***cis***$_{anti}$, no bond path and no bond critical point was found between the Si and the H atom excluding any direct Si···H bonding interaction (Fig. 12, left).

In comparison, for ***cis***$_{syn}$ a bond path with a bond critical point was found between the Si and the H atom. In this case, the interatomic surfaces crossing the Mo–H and the Mo–Si bond paths meet the interatomic surface crossing the Si–H bond path at a ring critical point (rcp), that is closely located to the Si–H bond critical point (Fig. 12, right). The proximity of the ring and bond critical point of the Si–H bond, as well as the similar values of the electron density at these points indicate a very weak direct Si···H interaction, which is also reflected in the low value of the energy density (Table 3).

Further information on the Si···H interaction in ***cis***$_{anti}$ and ***cis***$_{syn}$ was obtained from the sign and magnitude of the $^{29}$Si,$^{1}$H spin–spin coupling constant. One bond Si,H coupling constants ($^{1}J$(Si,H)) have negative signs due to the negative gyromagnetic ratio of the $^{29}$Si nucleus and range from *ca.* (−150)–(−400) Hz in silanes and transition metal hydrosilyl complexes, where only 2c–2e [TM-SiHRR′] interactions are present.[127,128] In comparison, two-bond (geminal) coupling constants ($^{2}J$(Si,H)) in silanes[127,129] and transition metal silyl hydrides, as

Table 3 Results of the AIM analyses of ***cis***$_{anti}$ and ***cis***$_{syn}$; values are given at the respective bond critical point ($r_{bcp}$) of each A–B bond and the ring critical point (rcp) of ***cis***$_{syn}$: electron density ($\rho$), Laplacian of the electron density $\nabla^2\rho$, relative kinetic energy density $\left(\frac{G}{\rho}\right)$, relative total energy density $\left(\frac{H}{\rho}\right)$ and bond ellipticity ($\varepsilon$); the position of the bcp is given in %, whereby a value larger than 50% means that the bcp is further away from atom A

| A–B | %A | %B | $\rho(r_{bcp})$/eÅ$^{-3}$ | $\nabla^2\rho(r_{bcp})$/eÅ$^{-5}$ | $\frac{G}{\rho}(r_{bcp})/E_H e^{-1}$ | $\frac{H}{\rho}(r_{bcp})/E_H e^{-1}$ | $\varepsilon$ |
|---|---|---|---|---|---|---|---|
| ***cis***$_{anti}$ | | | | | | | |
| Mo–H | 65 | 35 | 0.732 | 2.157 | 0.674 | −0.468 | 0.115 |
| Mo–Si | 53 | 47 | 0.598 | 0.113 | 0.478 | −0.465 | 0.279 |
| ***cis***$_{syn}$ | | | | | | | |
| Mo–H | 65 | 35 | 0.686 | 2.917 | 0.727 | −0.429 | 0.185 |
| Mo–Si | 53 | 47 | 0.587 | 0.230 | 0.485 | −0.458 | 0.028 |
| Si–H | 57 | 43 | 0.478 | 0.023 | 0.344 | −0.341 | 1.267 |
| rcp | 17.8 pm[a] | | 0.474[b] | 1.508[b] | 0.516[b] | −0.294[b] | — |

[a] Distance between the rcp and the bcp(Si–H). [b] Values at the rcp.

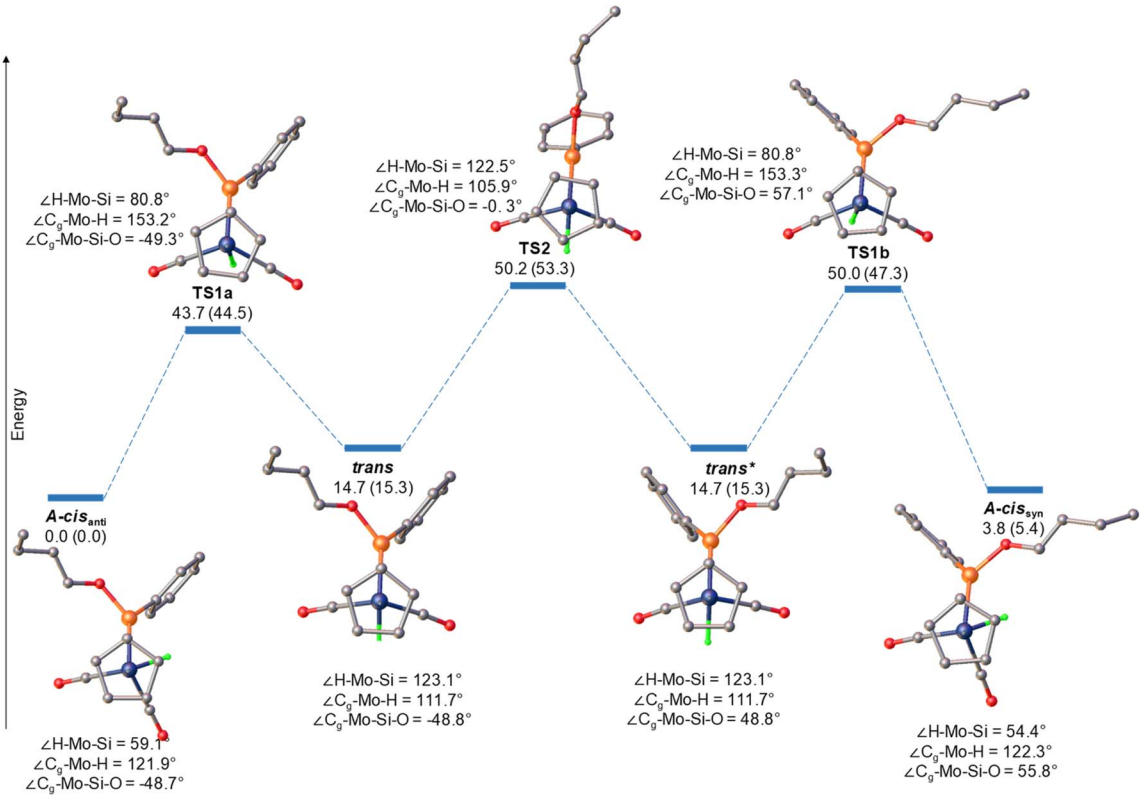


Fig. 13 Reaction profile for the diastereomerization of ***A-cis***$_{anti}$ to ***A-cis***$_{syn}$; Olex plots of the calculated structures of ***A-cis***$_{anti}$, ***A-cis***$_{syn}$, the transition states (**TS1a**, **TS2** and **TS1b**) and the intermediates ***trans*** and ***trans**** (top views) with their relative zero-point vibrational energy corrected inner energies $\Delta U$(0 K) (kJ mol$^{-1}$) and standard free energies $\Delta G°$ (kJ mol$^{-1}$) (values in parentheses).

$[Fe(H)(SiCl_3)(CO)_4]$,[130,131] usually have positive signs and much smaller values (*ca.* 5–25 Hz). The calculated $^{29}$Si,$^{1}$H coupling constant of ***cis***$_{anti}$ has a positive sign (+27.7 Hz), as expected for a $^{2}J$(Si,H) coupling, and excludes a direct Si···H interaction in ***cis***$_{anti}$ in line with the AIM results. In comparison, the calculated $^{29}$Si-$^{1}$H coupling constant of ***cis***$_{syn}$, where the Si–H distance (195.9 pm) is shorter by 14 pm than in ***cis***$_{anti}$ has a negative value (−7.2 Hz). Notably, the same trend and a sign change of the $J$(Si,H) coupling from plus to minus was observed in transition metal silyl hydride complexes upon decreasing the Si–H distance leading to an increased direct M–Si···H bonding interaction and finally to non classical hydrosilane complexes.[131,132] In the case of ***cis***$_{syn}$ the negative sign of the $J$(Si,H) coupling and its small absolute value suggests in combination with the AIM results a direct, weak Si···H bonding interaction. Notably, the experimental value of the $J$(Si,H) coupling constant of **3-Mo** (22 Hz) agrees well with the calculated value of $J(Si,H)_{th}$ (18 Hz) obtained from the following equation,

$$J(Si,H)_{th}\ (\mathbf{3\text{-}Mo}) = x_1 \times J(Si,H)_{th}(\boldsymbol{cis}_{anti}) + x_2 \times J(Si,H)_{th}(\boldsymbol{cis}_{syn})$$

where $x_1$ and $x_2$ are the mole fractions of ***cis***$_{anti}$ and ***cis***$_{syn}$, respectively, obtained from the experimental IR spectrum of **3-Mo** ($K_{exp}$ = 2.6, *vide supra*), and $J(Si,H)_{th}$(***cis***$_{anti}$) and $J(Si,H)_{th}$(***cis***$_{syn}$) are the calculated Si,H coupling constants of ***cis***$_{anti}$ and of ***cis***$_{syn}$, respectively.

As outlined above, the experimental and theoretical IR studies of **3-Mo** indicate the presence of two isomers (***cis***$_{anti}$ and ***cis***$_{syn}$) in solution. In comparison, the $^{1}$H, $^{13}$C{$^{1}$H} and $^{29}$Si{$^{1}$H} NMR spectra of **3-Mo** show only one set of signals, the number and multiplicity of which indicate a time-averaged $C_s$-symmetric structure in solution with the symmetry plane passing through the silylidene ligand plane and bisecting the $Cp^*Mo(CO)_2$ fragment and the Tbb ring plane. For example, the $^{1}$H NMR spectrum of **3-Mo** in ($D_6$)benzene at 298 K shows only one Mo–H resonance at $\delta = -7.42$ ppm, which is flanked by $^{29}$Si satellites due to $^{29}$Si-$^{1}$H spin–spin coupling (Fig. 9c). Furthermore, the $^{29}$Si{$^{1}$H} NMR spectrum of **3-Mo** shows only one $^{29}$Si resonance for the Mo=*Si* group at $\delta = 215.8$ ppm instead of the expected two resonances, and two $^{29}$Si resonances for the $SiMe_3$ groups instead of the four signals expected for each of the isomers ***cis***$_{anti}$ and ***cis***$_{syn}$ in case of a hindered rotation of the Tbb substituent around the Si–$C_{Tbb}$ bond (Fig. 9d). Finally, the $^{13}$C{$^{1}$H} spectrum of **3-Mo** shows only one signal for the two CO ligands at $\delta = 235.0$ ppm (Fig. 9e). This is quite different from what would be expected for the static structures of the $C_1$-symmetric isomers ***cis***$_{anti}$ and ***cis***$_{syn}$, for which two singlets should be observed for the diastereotopic CO ligands, respectively.

All NMR features of **3-Mo** indicate that in solution, a rapid equilibration of the isomers ***cis***$_{anti}$ and ***cis***$_{syn}$ occurs, which proceeds *via* a $C_s$-symmetric state. This process is too fast to be resolved on the NMR time scale ($10^{1}$–$10^{-6}$ s). The two isomers

can be observed though by IR spectroscopy due to the faster time scale of this method ($10^{-11}$–$10^{-14}$ s). This was verified by quantum chemical studies suggesting a reaction path *via* two enantiomeric *trans* intermediates for the interconversion of ***cis***$_{\mathbf{anti}}$ and ***cis***$_{\mathbf{syn}}$ (Fig. 13).

In the first step ***A-cis***$_{\mathbf{anti}}$ isomerizes to the *trans* diastereomer ***trans*** by migration of the H ligand from the *cis* to the *trans* position to the silylidene ligand (Fig. 13). A closer look at the trajectory connecting ***A-cis***$_{\mathbf{anti}}$ to ***trans*** *via* the transition state **TS1a** shows that the H–Mo–Si angle and the Si–H distance increase continuously along the path from ***A-cis***$_{\mathbf{anti}}$ to **trans**, while the $C_g$–Mo–H angle increases first from 121.9° (***A-cis***$_{\mathbf{anti}}$) to a maximum value in a pseudo-trigonal-bipyramidal structure, in which the Cp* and H ligands occupy nearly the apical positions, and then decreases over 153° in the transition state **TS1a** to 111.7° in the *trans* product. Remarkably, the tilted conformation of the silylidene ligand is maintained during the isomerization as shown by the dihedral angle $C_g$–Mo–Si–O making the *trans* product chiral (Fig. 13).

### 2.3 Reactions with 1,3 dipoles

Next, we investigated the reactivity of silylidyne complex **1-Mo** with 1,3-dipoles. Diazoalkanes form together with organic azides and nitrous oxide an important class of 1,3-dipoles, the diazonium betaines, according to Huisgen's definition.[133] Their 1,3-cycloaddition reactions with alkynes are very important in heterocycle synthesis and have been extensively studied in experiment and theory.[134,135] In comparison, reactivity studies towards the heavier alkyne congeners RE≡ER ($E$ = Si–Pb) are very scarce[136] and reactions of diazoalkanes with transition metal tetrylidyne complexes have not been explored. Earlier work in our group has shown that the germylidyne complex [Cp(CO)$_2$Mo≡Ge–Ar$^{Mes}$] reacts rapidly and selectively with two equivalents of trimethylsilyldiazomethane to afford a 1-metalla-3-germabicyclo[1.1.0]cyclobutane (eqn (5)).[137] The reaction proceeds presumably *via* two sequential, regioselective [2 + 3] cycloaddition and $N_2$ elimination steps resulting in an overall double carbene transfer to the Mo≡Ge bond.

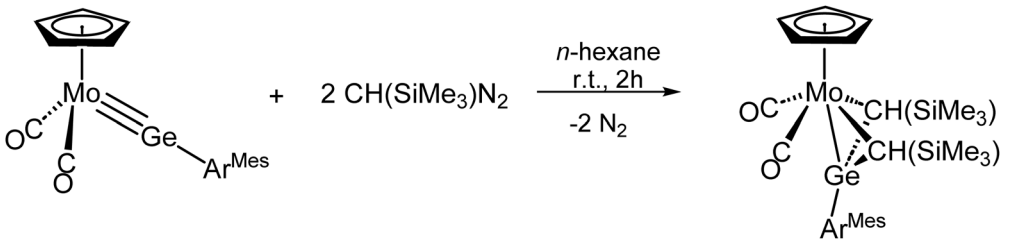


(5)

In the next step the ***trans*** isomer transforms to its conformational enantiomer ***trans**** *via* the $C_s$ symmetric transition state **TS2**. A look at the trajectory connecting ***trans*** to ***trans**** shows that the reaction path involves a rotation of the silylidene ligand around the Mo=Si bond as shown by the change in the dihedral angle $C_g$–Mo–Si–O from −48.8° in ***trans*** to +48.8° in ***trans****. The silylidene adopts in the transition state **TS2** an upright conformation with the OR substituent pointing towards the Cp* group ($\angle$($C_g$–Mo–Si–O) = −0.3°). In the final step ***trans**** converts to the *cis* diastereomer ***A-cis***$_{\mathbf{syn}}$ by migration of the H ligand from the *trans* to the *cis* position relative to the silylidene ligand. The reaction path is similar to the one that leads the ***trans*** intermediate back to ***A-cis***$_{\mathbf{anti}}$. It is noteworthy, that the isomerization pathway leading to equilibration between ***A-cis***$_{\mathbf{anti}}$ and its diastereomer ***A-cis***$_{\mathbf{syn}}$ in solution (and in the same way between ***C-cis***$_{\mathbf{anti}}$ and ***C-cis***$_{\mathbf{syn}}$) does not involve a change in the metal configuration. The calculated free energies of activation range from 32 to 44.5 kJ mol$^{-1}$ for the forward reaction and from 29.2 to 41.9 kJ mol$^{-1}$ for the backward reaction suggesting that the process may be detectable by NMR spectroscopy at low-temperature. However, the $^1$H NMR (300.1 MHz) spectrum of **3-Mo** in ($D_8$)toluene showed no significant change up to 193 K and the $^{13}$C {$^1$H} NMR spectrum (75.47 MHz) of **3-Mo** at 193 K only showed an incipient broadening of the CO signal at $\delta$ = 236.2 ppm ($\Delta\nu_{1/2}$ = 10.3 Hz) (Fig. 9e) indicating that the process at 193 K is still too fast on the NMR time scale (Fig. 14).

The silylidyne complex **1-Mo** reacts also rapidly with two equivalents of trimethylsilyldiazomethane. However, no $N_2$ elimination is observed in this reaction leading selectively to the orange-red, highly air sensitive complex **4-Mo** (eqn (6)). The reaction has no precedent in alkyne chemistry and probably involves a double [2 + 1] cycloaddition to the terminal N atom of the diazoalkane leading finally to a cleavage of the Mo–Si bond. It is reminiscent of the reaction of the disilene Mes$_2$Si=SiMes$_2$[138] and phosphasilenes[139] with aryldiazoalkanes. Compound **4-Mo** is the first silaamidinato complex reported in the literature, whereas metal amidinates are a well-studied class of compounds.[140–142]

The molecular structure of **4-Mo** shows a planar four-membered metallacycle with an acute angle at the Mo ($\angle$N1–Mo–N3 = 67.0(1)°) and a transannular Mo···Si distance of 296.1(1) pm, which is *ca.* 43 pm longer than the Mo–Si single bond of **2-Mo**, suggesting that there is no direct Mo–Si bonding interaction in **4-Mo** (Fig. 14). The silicon atom is trigonal planar coordinated and the endocyclic Si–N bond lengths of 165.8 and 165.1 pm are in between those of Si=N double bonds (153–163 pm)[143] and Si–N single bonds (170–175 pm),[144] suggesting a 3c-2π delocalization over the NSiN moiety. The exocyclic N–N and C=N bond lengths are in the common range of N–N single and C=N double bonds of azines R$_2$C=N–N=CR$_2$, respectively.[145] **4-Mo** displays in the $^{29}$Si NMR spectrum a resonance signal at $\delta$ = 31.8 ppm.

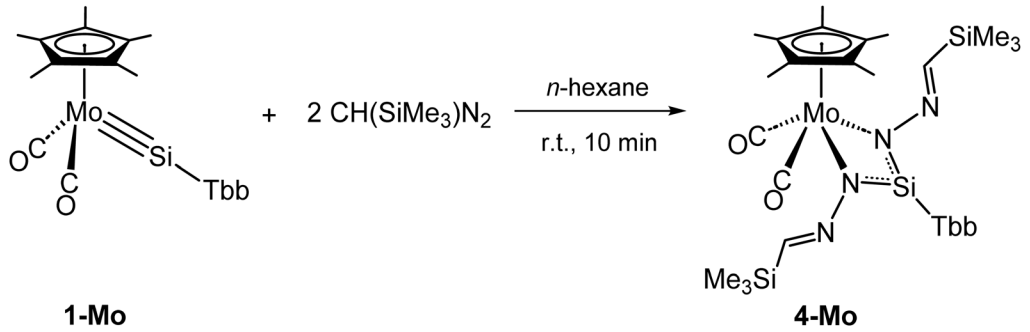


(6)

**1-Mo** **4-Mo**

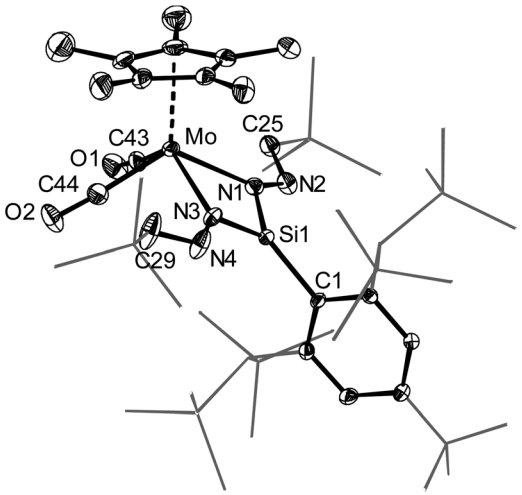


Fig. 14 DIAMOND plot of the molecular structure of **4-Mo**. Thermal ellipsoids are set at 30% probability, hydrogen atoms were omitted and the substituents of the Tbb group are presented as wireframe for the sake of clarity. Selected distances (pm) and bond angles (°): Mo···Si1 296.1(1), Mo–N1 224.5(4), Mo–N3 222.7(4), Si1–N1 165.8(4), Si1–N3 165.1(4), Si1–C1 183.6(4), N1–N2 138.2(6), N3–N4 137.4(6), N2–C25 129.2(7), N4–C29 129.0(8), N1–Mo–N3 67.0(1), N1–Si1–N3 96.4(2), N1–Si1–C1 130.8(2), N3–Si1–C1 132.6(2).

Organic azides are also potent 1,3-dipoles and their [3 + 2] cycloaddition with alkynes is one of the most important reactions in click chemistry.[134] Few [3 + 2] cycloadditions of organic azides with Fischer-type carbyne complexes were also reported leading exclusively to 2*H*-1-metalla-2,3,4-triazoles (**e**, Fig. 15a).[82,146] In comparison, reaction of **1-Mo** with $MesN_3$ in *n*-hexane at room temperature yields by $N_2$ elimination the $\eta^2$-silaiminoacyl complex **5-Mo** (eqn (7)).

The following reaction pathway can be proposed for the formation of **5-Mo** reflecting the $Mo^{(\delta-)}{\equiv}Si^{(\delta+)}$ bond polarity. In the first step, a [3 + 2] cycloaddition of $MesN_3$ with **1-Mo** gives regioselectively the 4*H*-1-metalla-5-sila-2,3,4-triazole **f** (Fig. 15b). In this reaction, the internal nucleophilic N atom of $MesN_3$ attacks the electrophilic silicon atom of **1-Mo**, whereas the nucleophilic Mo center of **1-Mo** gets attached to the electrophilic terminal N atom of $MesN_3$. In the next step, ring opening by cleavage of the $N^{Mes}$–N bond leads to the $\eta^1$-silaiminoacyl-dinitrogen complex **g**, which cleaves off $N_2$ by coordination of the imino nitrogen to the metal center, yielding **5-Mo** (Fig. 15b). It is noteworthy, that the regioselectivity of the [3 + 2] cycloaddition of the carbyne complexes is opposite to that of the silylidyne complex **1-Mo** and that formation of the 4*H*-1-metalla-2,3,4-triazoles **e′**, the carbon analogs of **f**, is kinetically and thermodynamically unfavorable according to quantum chemical calculations.[147]

**5-Mo** was isolated as an air sensitive, black, stable solid, that decomposes upon melting at 176 °C. The molecular structure of the "four-legged piano stool" complex **5-Mo** features a three membered metallaazasilirene ring (Fig. 16). The Mo–Si (239.77(8)°pm) and Si–N (161.5(3)°pm) bond lengths compare well with those recently reported for the complex $[MoCp^*(CO)_2(\kappa^2Si,N\text{–}Si(Eind)NSiMe_3)]$[60] and lie in the upper limit of reported Mo═Si (228.8(2)–238.72(7) pm)[38,48,60,66,119,120] and Si═N (153.3(2) pm–162.6(1) pm)[143] bond lengths, respectively.

These data can be rationalized with the two resonances structures **I** and **II** for the silaiminoacyl ligand (Fig. 17). **5-Mo** shows a characteristic deshielded $^{29}Si$ NMR signal at $\delta = 142.9$ ppm. Notably, **5-Mo** is stereochemically not rigid in solution as evidenced by the single $^{13}C$ NMR signal observed for the

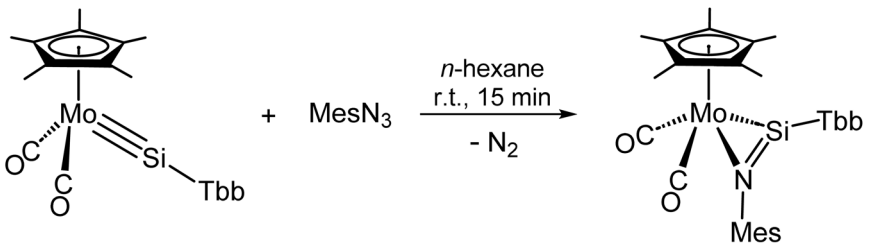


(7)

**1-Mo** **5-Mo**

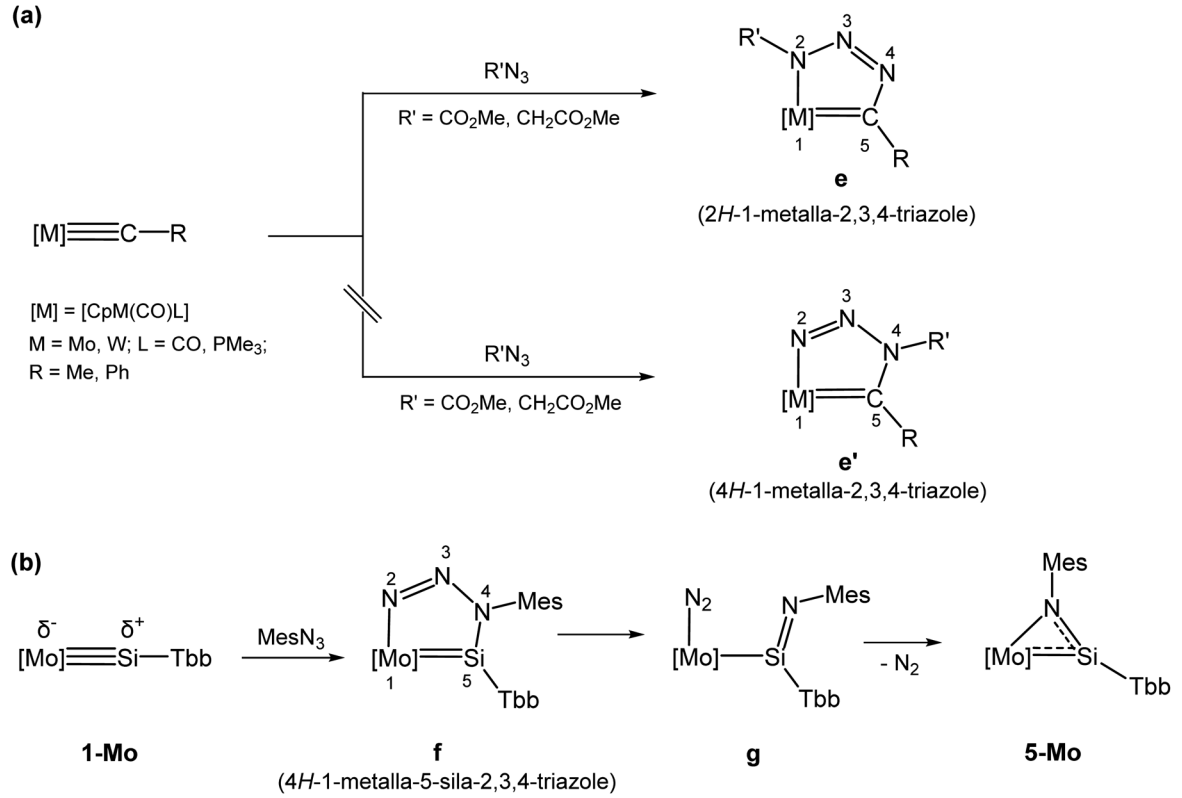


Fig. 15 (a) [3 + 2] cycloaddition of organic azides with metal carbyne complexes; (b) proposed pathway for the reaction of **1-Mo** with $MesN_3$.

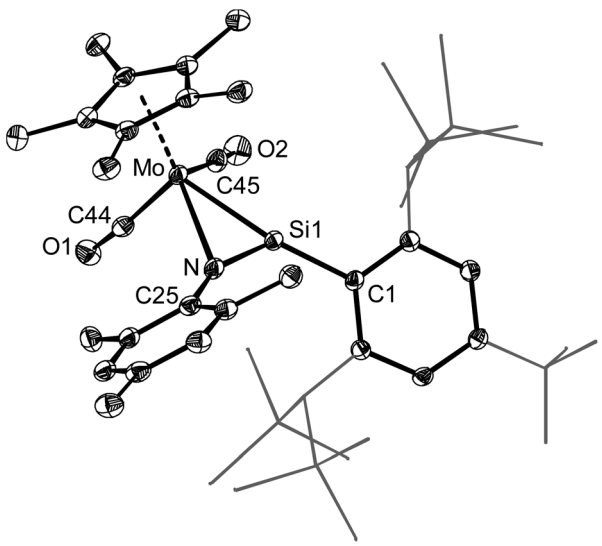


Fig. 16 DIAMOND plot of the molecular structure of **5-Mo**. Thermal ellipsoids are set at 30% probability, hydrogen atoms were omitted and the substituents of the Tbb group are presented as wireframe for the sake of clarity. Selected bond lengths (pm) and bond angles (°): Mo–Si1 239.77(8), Mo–N 239.1(2), Mo–C44 196.3(3), Mo–C45 195.0(3), Si1–N 161.5(3), Si1–C1 187.0(3), N–C25 140.2(4), Mo–Si1–C1 161.92(9), Mo–Si1–N 70.07(8), Si1–Mo–N 39.41(7), N–Si1–C1 126.4(1), Mo–N–Si1 70.52(9), Mo–N–C25 135.5(2), Si1–N–C25 151.8(2).

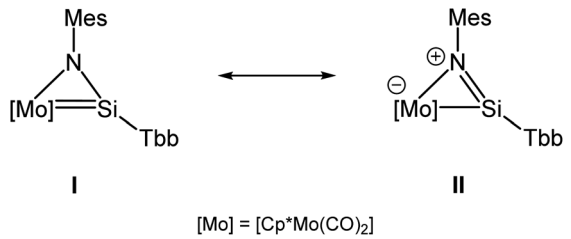


Fig. 17 Resonance structures of **5-Mo**.

diastereotopic CO ligands or the single $^1H$ and $^{13}C$ NMR signals observed for the diastereotopic $SiMe_3$ groups of the Tbb substituent (ESI, Chapter 2.8†). The stereomutation presumably involves a 180° rotation of the silaiminoacyl ligand about an axis connecting the Mo atom with the middle point of the Si═N bond and leads to the enantiomer of **5-Mo**, in which Si and N atoms have swapped coordination sites. The enantiomerization is too fast on the NMR time scale even at 223 K ($^1H$ NMR, 300.1 MHz, ($D_8$)toluene) and has a lower activation barrier than the same process observed for the isoelectronic iminoacyl complexes $[MoCp^*(CO)_2(\eta^2C,N\text{–}C(R)NEt)]$ (R = Me, Et).[148]

## 3. Conclusion

The series of novel reactions of the complexes $[Cp^*(CO)_2M{\equiv}Si\text{–}Tbb]$ (M = Cr – W) presented in this work substantiate the synthetic potential of metal-silicon triple bonds. The different regiochemistry of M≡Si and M≡C bonds and the growing

number of isolable silylidyne complexes with a variable metal d configuration and coordination number open many perspectives and objectives for a flourishing field of silicon-directed metal chemistry.

## Data availability

The ESI† (.pdf) contains the syntheses, the spectroscopic data, the IR and NMR spectra, the crystallographic data and the structure refinement parameters of **1-Cr** – **5-Mo**, and details of the quantum chemical calculations of **3-Mo**. The ESI† (.txt) contains the cartesian coordinates of the calculated structures: deposition numbers CCDC-2421358 (**1-Cr**), CCDC-2421359 (**1-Mo**), CCDC-2421360 (**1-W**), CCDC-2421361 (**2-Mo**), CCDC-2421362 (**2-W·(toluene)**) CCDC-2421363 (**3-Mo**), CCDC-2421364 (**4-Mo**) and CCDC-2421365 (**5-Mo**) contain the supplementary crystallographic data for this paper. These data are provided free of charge by the joint Cambridge Crystallographic Data Centre and Fachinformationszentrum Karlsruhe Access Structures service.

## Author contributions

A. C. F. designed and directed the project. K. T. prepared and characterized the compounds, analyzed the data, and wrote the first draft. G. S. performed the theoretical calculations and SCXRD studies. U. D. helped with the data analysis. A. C. F. revised and finalized the manuscript. All authors discussed the results and reviewed the manuscript.

## Conflicts of interest

The authors declare no conflict of interest.

## Acknowledgements

We thank the Rheinische Friedrich-Wilhelms Universität Bonn for the financial support of this work. We also thank S. Henn for preliminary experimental work and Mrs K. Kühnel-Lysek, Mrs C. Rödde and Dipl.-Ing. K. Prochnicki for technical support.

## References

1 E. O. Fischer, *Angew. Chem., Int. Ed.*, 1974, **86**, 651–663.
2 E. O. Fischer, in *Advances in Organometallic Chemistry*, ed. F. G. A. Stone and R. West, Elsevier, 1976, vol. 14, pp. 1–32.
3 F. G. A. Stone, *Angew. Chem., Int. Ed. Engl.*, 1984, **23**, 89–99.
4 R. R. Schrock, *Acc. Chem. Res.*, 1986, **19**, 342–348.
5 H. P. Kim and R. J. Angelici, in *Advances in Organometallic Chemistry*, ed. B. W. O'Malley, Elsevier, 1987, vol. 27, pp. 51–111.
6 A. Mayr and H. Hoffmeister, in *Advances in Organometallic Chemistry*, ed. F. G. A. Stone and R. West, Elsevier, 1991, vol. 32, pp. 227–324.
7 R. R. Schrock, *Chem. Rev.*, 2002, **102**, 145–180.
8 R. R. Schrock, *Angew. Chem., Int. Ed.*, 2006, **45**, 3748–3759.
9 M. Cui and G. Jia, *J. Am. Chem. Soc.*, 2022, **144**, 12546–12566.
10 H. Fischer, E. O. Fischer, P. Hofmann, F. R. Kreissl, R. R. Schrock, U. Schubert and K. Weiss, *Carbyne complexes*, VCH publishers, New York, 1988, ISBN: 0-89573-849-X.
11 E. O. Fischer, G. Kreis, C. G. Kreiter, J. Müller, G. Huttner and H. Lorenz, *Angew. Chem., Int. Ed. Engl.*, 1973, **12**, 564–565.
12 A. Fürstner, *Angew. Chem., Int. Ed.*, 2013, **52**, 2794–2819.
13 H. Ehrhorn and M. Tamm, *Chem.–Eur. J.*, 2019, **25**, 3190–3208.
14 S. Huang, Z. Lei, Y. Jin and W. Zhang, *Chem. Sci.*, 2021, **12**, 9591–9606.
15 D. Lee, I. Volchkov and S. Y. Yun, in *Organic Reactions*, ed. S. E. Denmark, Wiley, 2020, pp. 613–931.
16 A. C. Filippou, D. Hoffmann and G. Schnakenburg, *Chem. Sci.*, 2017, **8**, 6290–6299.
17 P. Ghana, M. I. Arz, G. Schnakenburg, M. Straßmann and A. C. Filippou, *Organometallics*, 2018, **37**, 772–780.
18 L. R. Maurer, J. Rump and A. C. Filippou, *Inorganics*, 2023, **11**, 129, and references therein.
19 R. S. Simons and P. P. Power, *J. Am. Chem. Soc.*, 1996, **118**, 11966–11967.
20 L. Pu, B. Twamley, S. T. Haubrich, M. M. Olmstead, B. V. Mork, R. S. Simons and P. P. Power, *J. Am. Chem. Soc.*, 2000, **122**, 650–656.
21 E. Rivard and P. P. Power, *Inorg. Chem.*, 2007, **46**, 10047–10064.
22 A. C. Filippou, A. I. Philippopoulos, P. Portius and D. U. Neumann, *Angew. Chem., Int. Ed.*, 2000, **39**, 2778–2781.
23 A. C. Filippou, P. Portius and A. I. Philippopoulos, *Organometallics*, 2002, **21**, 653–661.
24 A. C. Filippou, A. I. Philippopoulos, P. Portius and G. Schnakenburg, *Organometallics*, 2004, **23**, 4503–4512.
25 A. C. Filippou, G. Schnakenburg, A. I. Philippopoulos and N. Weidemann, *Angew. Chem., Int. Ed.*, 2005, **44**, 5979–5985.
26 A. C. Filippou, N. Weidemann, A. I. Philippopoulos and G. Schnakenburg, *Angew. Chem., Int. Ed.*, 2006, **45**, 5987–5991.
27 A. C. Filippou, P. Portius, A. I. Philippopoulos and H. Rohde, *Angew. Chem., Int. Ed.*, 2003, **42**, 445–447.
28 A. C. Filippou, A. I. Philippopoulos and G. Schnakenburg, *Organometallics*, 2003, **22**, 3339–3341.
29 H. Rohde, M. Menzel, F. Renz and A. C. Filippou, *Hyperfine Interact.*, 2008, **185**, 129–132.
30 A. C. Filippou, H. Rohde and G. Schnakenburg, *Angew. Chem., Int. Ed.*, 2004, **43**, 2243–2247.
31 A. C. Filippou, N. Weidemann, G. Schnakenburg, H. Rohde and A. I. Philippopoulos, *Angew. Chem., Int. Ed.*, 2004, **43**, 6512–6516.
32 A. C. Filippou, N. Weidemann and G. Schnakenburg, *Angew. Chem., Int. Ed.*, 2008, **47**, 5799–5802.
33 S. Saini, A. Agarwal and S. K. Bose, *Dalton Trans.*, 2020, **49**, 17055–17075.
34 H. Hashimoto and K. Nagata, *Chem. Lett.*, 2021, **50**, 778–787.
35 T. J. Hadlington, *Chem. Soc. Rev.*, 2024, **53**, 9738–9831.

36 A. L. Allred and E. G. Rochow, *J. Inorg. Nucl. Chem.*, 1958, **5**, 269–288.
37 S. D. Grumbine, R. K. Chadha and T. D. Tilley, *J. Am. Chem. Soc.*, 1992, **114**, 1518–1520.
38 B. V. Mork and T. D. Tilley, *Angew. Chem., Int. Ed.*, 2003, **42**, 357–360.
39 A. C. Filippou, O. Chernov and G. Schnakenburg, *Angew. Chem., Int. Ed.*, 2009, **48**, 5687–5690.
40 R. S. Ghadwal, H. W. Roesky, S. Merkel, J. Henn and D. Stalke, *Angew. Chem., Int. Ed.*, 2009, **48**, 5683–5686.
41 A. C. Filippou, O. Chernov, B. Blom, K. W. Stumpf and G. Schnakenburg, *Chem.–Eur. J.*, 2010, **16**, 2866–2872.
42 A. C. Filippou, O. Chernov and G. Schnakenburg, *Chem.–Eur. J.*, 2011, **17**, 13574–13583.
43 A. C. Filippou, Y. N. Lebedev, O. Chernov, M. Straßmann and G. Schnakenburg, *Angew. Chem. Int. Ed.*, 2013, **125**, 7112–7116.
44 N. Wiberg, W. Niedermayer, G. Fischer, H. Nöth and M. Suter, *Eur. J. Inorg. Chem.*, 2002, 1066–1070.
45 Y. Sugiyama, T. Sasamori, Y. Hosoi, Y. Furukawa, N. Takagi, S. Nagase and N. Tokitoh, *J. Am. Chem. Soc.*, 2006, **128**, 1023–1031.
46 K. Suzuki, T. Matsuo, D. Hashizume and K. Tamao, *J. Am. Chem. Soc.*, 2011, **133**, 19710–19713.
47 T. Agou, N. Hayakawa, T. Sasamori, T. Matsuo, D. Hashizume and N. Tokitoh, *Chem.–Eur. J.*, 2014, **20**, 9246–9249.
48 A. C. Filippou, O. Chernov, K. W. Stumpf and G. Schnakenburg, *Angew. Chem., Int. Ed.*, 2010, **49**, 3296–3300.
49 O. Chernov, *Novel Molecular Si(II) Precursors for Synthesis of the First Compounds with Metal-Silicon Triple Bonds*, Dissertation, Rheinische Friedrich-Wilhelms-Universität Bonn, 2012, URN: **https://nbn-resolving.org/urn:nbn:de:hbz:5n-29944**.
50 A. C. Filippou, B. Baars, O. Chernov, Y. N. Lebedev and G. Schnakenburg, *Angew. Chem., Int. Ed.*, 2014, **53**, 565–570.
51 B. Baars, Synthese und Reaktivität von kationischen Metallosilylidinen und Metallosilylenen, PhD thesis, Rheinische Friedrich-Wilhelms-Universität Bonn, published in Mensch und Buch Verlag2017, ISBN: 978-3-86387-825-2.
52 P. Ghana, M. I. Arz, U. Chakraborty, G. Schnakenburg and A. C. Filippou, *J. Am. Chem. Soc.*, 2018, **140**, 7187–7198.
53 N. Wienkenhöver, 1,2-Dibromodisilenes: A Rich Source for Titanium Silylidyne Complexes, Acyclic Silylenes and Disilyne Dianions, PhD thesis, Rheinische Friedrich-Wilhelms-Universität Bonn, published in Mensch und Buch Verlag, 2017, ISBN: 978-3-86387-864-1.
54 I. Papazoglou, Unprecedented Tetrylidyne Complexes of Group 6 and 10 Metals, PhD thesis, Rheinische Friedrich-Wilhelms-Universität Bonn, published in Dr Hut Verlag, 2017, ISBN: 978-3-8439-3155-7.
55 A. Lülsdorf, Tetrylidin-Komplexe des Titans, PhD thesis, Rheinische Friedrich-Wilhelms-Universität Bonn, published in Mensch und Buch Verlag, Berlin, 2021, ISBN: 978-3-96729-134-6.
56 T. Deckstein and A. C. Filippou, $(PMe_3)_3Co{\equiv}SiTbb$: A Cobalt Silylidyne Complex via Metathetical Exchange of Cobalt-Tetrel Triple Bonds, in *10th European Silicon Days*, Toulouse, France, 2023.
57 P. G. Hayes, Z. Xu, C. Beddie, J. M. Keith, M. B. Hall and T. D. Tilley, *J. Am. Chem. Soc.*, 2013, **135**, 11780–11783.
58 T. Fukuda, T. Yoshimoto, H. Hashimoto and H. Tobita, *Organometallics*, 2016, **35**, 921–924.
59 T. Yoshimoto, H. Hashimoto, N. Hayakawa, T. Matsuo and H. Tobita, *Organometallics*, 2016, **35**, 3444–3447.
60 H. Hashimoto, K. Watanabe, T. Yoshimoto, N. Hayakawa, T. Matsuo and H. Tobita, *Chem.–Eur. J.*, 2023, **29**, e202302470.
61 M. Matsuoka, K. Nagata, R. Ohno, T. Matsuo, H. Tobita and H. Hashimoto, *Chem.–Eur. J.*, 2024, **30**, e202303765.
62 M. Lein, A. Szabó, A. Kovács and G. Frenking, *Faraday Discuss.*, 2003, **124**, 365–378.
63 N. Takagi, K. Yamazaki and S. Nagase, *Bull. Korean Chem. Soc.*, 2003, **24**, 832–836.
64 G. Schnakenburg, Quantenchemische Untersuchungen an Tetrela-Ylidin-Komplexen der 6, 8 und 9 Nebengruppe, PhD thesis, Rheinische Friedrich-Wilhelms-Universität Bonn, 2008.
65 P. R. Wosniok, *Beiträge zur Chemie und Reaktivitätsuntersuchung des ersten Silylidin-Komplexes* $Cp(CO)_2Mo{\equiv}Si(C_6H_3\text{-}2,6\text{-}Trip_2)$, Rheinische Friedrich-Wilhelms-Universität Bonn, Diplomarbeit, 2012.
66 A. C. Filippou, O. Chernov and G. Schnakenburg, *Angew. Chem., Int. Ed.*, 2011, **50**, 1122–1126.
67 A. Hassner, *J. Org. Chem.*, 1968, **33**, 2684–2686.
68 J. C. Jeffery, J. C. V. Laurie, I. Moore and F. G. A. Stone, *J. Organomet. Chem.*, 1983, **258**, C37–C40.
69 F. R. Kreissl, W. J. Sieber, H. Keller, J. Riede and M. Wolfgruber, *J. Organomet. Chem.*, 1987, **320**, 83–90.
70 A. C. Filippou, P. Portius, J. G. Winter and G. Kociok-Köhn, *J. Organomet. Chem.*, 2001, **628**, 11–24.
71 T. J. Katz, T. H. Ho, N. Y. Shih, Y. C. Ying and V. I. W. Stuart, *J. Am. Chem. Soc.*, 1984, **106**, 2659–2668.
72 T. M. Sivavec and T. J. Katz, *Tetrahedron Lett.*, 1985, **26**, 2159–2162.
73 L. M. Atagi and J. M. Mayer, *Organometallics*, 1994, **13**, 4794–4803.
74 H. Fischer and C. Troll, *J. Chem. Soc., Chem. Commun.*, 1994, 457–458.
75 A. Mayr, K. S. Lee and B. Kahr, *Angew. Chem., Int. Ed. Engl.*, 1988, **27**, 1730–1731.
76 J. H. Freudenberger and R. R. Schrock, *Organometallics*, 1986, **5**, 398–400.
77 R. Goller, U. Schubert and K. Weiss, *J. Organomet. Chem.*, 1993, **459**, 229–232.
78 M. Matsuoka, K. Nagata, R. Ohno, T. Matsuo and H. Hashimoto, *Chem. Lett.*, 2024, **53**, upae002.
79 P. Ghana, Synthesis, Characterization and Reactivity of Ylidyne and μ-Ylido Complexes Supported by Scorpionato Ligands, PhD thesis, Rheinische Friedrich-Wilhelms-Universität Bonn, Springer International Publishing AG, 2019, ISBN: 978-3-030-02624-0 978-3-030-02625-7.

80 P. Ghana, J. Rump, G. Schnakenburg, M. I. Arz and A. C. Filippou, *J. Am. Chem. Soc.*, 2021, **143**, 420–432.
81 A. C. Filippou, D. Wössner, G. Kociok-Köhn and I. Hinz, *J. Organomet. Chem.*, 1997, **541**, 333–343.
82 C. M. Stegmair, W. Schütt, W. Ullrich, P. Kiprof, J. Ostermeier and F. R. Kreißl, *J. Organomet. Chem.*, 1993, **447**, 251–257.
83 E. O. Fischer, T. L. Lindner and F. R. Kreissl, *J. Organomet. Chem.*, 1976, **112**, C27–C30.
84 E. O. Fischer, T. L. Lindner, G. Huttner, P. Friedrich, F. R. Kreißl and J. O. Besenhard, *Chem. Ber.*, 1977, **110**, 3397–3404.
85 E. Delgado, J. Hein, J. C. Jeffery, A. L. Ratermann, F. G. A. Stone and L. J. Farrugia, *J. Chem. Soc., Dalton Trans.*, 1987, 1191–1199.
86 H. Wadepohl, U. Arnold, H. Pritzkow, M. J. Calhorda and L. F. Veiros, *J. Organomet. Chem.*, 1999, **587**, 233–243.
87 J. C. Jeffery, F. Gordon, A. Stone and G. K. Williams, *Polyhedron*, 1991, **10**, 215–219.
88 P. Pyykkö, S. Riedel and M. Patzschke, *Chem.–Eur. J.*, 2005, **11**, 3511–3520.
89 J. Potenza, P. Giordano, D. Mastropaolo and A. Efraty, *Inorg. Chem.*, 1974, **13**, 2540–2544.
90 J.-S. Huang and L. F. Dahl, *J. Organomet. Chem.*, 1983, **243**, 57–68.
91 T. Sugahara, J.-D. Guo, D. Hashizume, T. Sasamori, S. Nagase and N. Tokitoh, *Dalton Trans.*, 2018, **47**, 13318–13322.
92 A. C. Filippou, W. Grünleitner, E. O. Fischer, W. Imhof and G. Huttner, *J. Organomet. Chem.*, 1991, **413**, 165–179.
93 A. C. Filippou and W. Grünleitner, *Z. Naturforschung B*, 1989, **44**, 1572–1580.
94 D. M. Tellers, S. J. Skoog, R. G. Bergman, T. B. Gunnoe and W. D. Harman, *Organometallics*, 2000, **19**, 2428–2432.
95 G. Frenking, I. Fernández, N. Holzmann, S. Pan, I. Krossing and M. Zhou, *JACS Au*, 2021, **1**, 623–645.
96 T. Mukaiyama, T. Fujisawa and T. Hyugaji, *Bull. Chem. Soc. Jpn.*, 1962, **35**, 687–690.
97 N. P. Marullo and E. H. Wagener, *J. Am. Chem. Soc.*, 1966, **88**, 5034–5035.
98 C. R. Flynn and J. Michl, *J. Org. Chem.*, 1974, **39**, 3442–3443.
99 D. Hoppe and L. Beckmann, *Liebigs Ann. Chem.*, 1980, **1980**, 1751–1764.
100 J. Kohn and R. Langer, *Biomaterials*, 1986, **7**, 176–182.
101 P. Adams and F. A. Baron, *Chem. Rev.*, 1965, **65**, 567–602.
102 X. Liu, X.-Q. Xiao, Z. Xu, X. Yang, Z. Li, Z. Dong, C. Yan, G. Lai and M. Kira, *Organometallics*, 2014, **33**, 5434–5439.
103 H.-W. Lerner, M. Bolte and M. Wagner, *Dalton Trans.*, 2017, **46**, 8769–8773.
104 A CSD survey gave 81 structures with Mo–Si single bonds and 89 structures with W–Si single bonds (coordination number of Si = 4). The mean and median values of the M–Si bond lengths were 254.2 and 255.6 pm (M = Mo) and 256.4 and 257.4 pm (M = W), respectively.
105 W. Beck, A. Melnikoff and R. Stahl, *Angew. Chem., Int. Ed. Engl.*, 1965, **4**, 692–693.
106 A. C. Filippou, J. G. Winter, M. Feist, G. Kociok-Köhn and I. Hinz, *Polyhedron*, 1998, **17**, 1103–1114.
107 A CSD search gave overall 11 structures of four-coordinate Si compounds featuring a siletane ring $Si(X^1)(X^2)C{=}Y$ ($X^1$, $X^2$, Y = NR, O).
108 T. Fukuda, H. Hashimoto, S. Sakaki and H. Tobita, *Angew. Chem., Int. Ed.*, 2016, **55**, 188–192.
109 K. Weiss, U. Schubert and R. R. Schrock, *Organometallics*, 1986, **5**, 397–398.
110 G. P. Mitchell and T. D. Tilley, *J. Am. Chem. Soc.*, 1997, **119**, 11236–11243.
111 M. Ochiai, H. Hashimoto and H. Tobita, *Organometallics*, 2012, **31**, 527–530.
112 H. Xie and Z. Lin, *Organometallics*, 2014, **33**, 892–897.
113 G. A. Olah, J. Nishimura and P. Kreienbuehl, *J. Am. Chem. Soc.*, 1973, **95**, 7672–7680.
114 Z. Karpas, W. J. Stevens, T. J. Buckley and R. Metz, *J. Phys. Chem.*, 1985, **89**, 5274–5278.
115 A. Schulz and A. Villinger, *Chem.–Eur. J.*, 2010, **16**, 7276–7281.
116 T. Hansen, P. Vermeeren, K. W. J. Zijderveld, F. M. Bickelhaupt and T. A. Hamlin, *Chem.–Eur. J.*, 2023, **29**, e202301308.
117 H. Hashimoto, M. Ochiai and H. Tobita, *J. Organomet. Chem.*, 2007, **692**, 36–43.
118 Oxysilylidene complexes are scarce and a CSD search shows that only three tungsten compounds have been structurally characterized.
119 B. V. Mork, T. D. Tilley, A. J. Schultz and J. A. Cowan, *J. Am. Chem. Soc.*, 2004, **126**, 10428–10440.
120 M. Hirotsu, T. Nunokawa and K. Ueno, *Organometallics*, 2006, **25**, 1554–1556.
121 A. J. Schultz, K. L. Stearley, J. M. Williams, R. Mink and G. D. Stucky, *Inorg. Chem.*, 1977, **16**, 3303–3306.
122 L. Brammer, D. Zhao, R. M. Bullock and R. K. McMullan, *Inorg. Chem.*, 1993, **32**, 4819–4824.
123 P. P. Gaspar, A. M. Beatty, T. Chen, T. Haile, D. Lei, W. R. Winchester, J. Braddock-Wilking, N. P. Rath, W. T. Klooster, T. F. Koetzle, S. A. Mason and A. Albinati, *Organometallics*, 1999, **18**, 3921–3932.
124 M. Grellier, T. Ayed, J.-C. Barthelat, A. Albinati, S. Mason, L. Vendier, Y. Coppel and S. Sabo-Etienne, *J. Am. Chem. Soc.*, 2009, **131**, 7633–7640.
125 M. Mantina, A. C. Chamberlin, R. Valero, C. J. Cramer and D. G. Truhlar, *J. Phys. Chem. A*, 2009, **113**, 5806–5812.
126 J. Y. Corey, *Chem. Rev.*, 2011, **111**, 863–1071.
127 J. Schraml and J. M. Bellama, in *Determination of Organic Structures by Physical Methods*, ed. F. C. Nachod, J. J. Zuckerman and E. W. Randall, Academic Press, New York, vol. 6, 1976, pp. 203–269, ISBN: 978-0-323-14920-4.
128 J. Y. Corey and J. Braddock-Wilking, *Chem. Rev.*, 1999, **99**, 175–292.
129 W. McFarlane, *J. Chem. Soc. A*, 1967, 1275–1276.
130 D. L. Lichtenberger, *Organometallics*, 2003, **22**, 1599–1602.
131 P. Meixner, K. Batke, A. Fischer, D. Schmitz, G. Eickerling, M. Kalter, K. Ruhland, K. Eichele, J. E. Barquera-Lozada,

N. P. M. Casati, F. Montisci, P. Macchi and W. Scherer, *J. Phys. Chem. A*, 2017, **121**, 7219–7235.
132 W. Scherer, P. Meixner, K. Batke, J. E. Barquera-Lozada, K. Ruhland, A. Fischer, G. Eickerling and K. Eichele, *Angew. Chem., Int. Ed.*, 2016, **55**, 11673–11677.
133 R. Huisgen, in *1,3 Dipolar Cycloaddition Chemistry*, ed. A. Padwa, John Wiley & Sons, New York, vol. 1, 1984, pp. 1–176, ISBN: 978047108364.
134 H. C. Kolb, M. G. Finn and K. B. Sharpless, *Angew. Chem., Int. Ed.*, 2001, **40**, 2004–2021.
135 D. H. Ess and K. N. Houk, *J. Am. Chem. Soc.*, 2008, **130**, 10187.
136 C. Cui, M. M. Olmstead, J. C. Fettinger, G. H. Spikes and P. P. Power, *J. Am. Chem. Soc.*, 2005, **127**, 17530–17541.
137 K. W. Stumpf, Germyliden- und Germylidin-Komplexe des Molybdäns, PhD thesis, Rheinische Friedrich-Wilhelms-Universität Bonn, published in Dr Hut Verlag, München, 2014, ISBN: 978-3-8439-1849-7.
138 H. Piana and U. Schubert, *J. Organomet. Chem.*, 1988, **348**, C19–C21.
139 M. Driess and H. Pritzkow, *Angew. Chem. Int. Ed. Engl.*, 1992, **31**, 751–753.
140 J. Barker and M. Kilner, *Coord. Chem. Rev.*, 1994, **133**, 219–300.
141 M. P. Coles, *Dalton Trans.*, 2006, 985.
142 S. Collins, *Coord. Chem. Rev.*, 2011, **255**, 118–138.
143 A CSD survey gave 17 structures of silaimines. The Si═N bond lengths ranged from 153.3(2) pm to 162.6(1) pm with a mean and median value of 157.5 and 157.3 pm, respectively.
144 W. S. Sheldrick, in *The Chemistry of Organic Silicon Compounds, Part 1*, ed. S. Patai and Z. Rappoport, John Wiley & Sons, 1989, pp. 227–303, ISBN: 0-471-91441-X.
145 D. D. Choytun, L. D. Langlois, T. P. Johansson, C. L. B. Macdonald, G. W. Leach, N. Weinberg and J. A. C. Clyburne, *Chem. Commun.*, 2004, 1842–1843.
146 C. M. Stegmair, W. Ullrich, W. Schütt, P. Kiprof and F. R. Kreißl, *Chem. Ber.*, 1992, **125**, 1571–1573.
147 Q. Zhu, S. Chen, F. Xu and J. Zhu, *Inorg. Chem.*, 2020, **59**, 7318–7324.
148 A. C. Filippou, W. Grünleitner and C. Völkl, *J. Organomet. Chem.*, 1991, **413**, 181–203.